Atmospheric
Measurement
Techniques

Aerosol optical depth comparison between GAW-PFR and AERONET-Cimel radiometers from long-term (2005–2015) 1 min synchronous measurements

Emilio Cuevas[1], Pedro Miguel Romero-Campos[1], Natalia Kouremeti[2], Stelios Kazadzis[2], Petri Räisänen[3], Rosa Delia García[4,1], Africa Barreto[5,1,4], Carmen Guirado-Fuentes[4,1], Ramón Ramos[1], Carlos Toledano[4], Fernando Almansa[5,1,4], and Julian Gröbner[2]

[1]Izaña Atmospheric Research Center (IARC), State Meteorological Agency (AEMET), Santa Cruz de Tenerife, Spain
[2]Physikalisch-Meteorologisches Observatorium Davos, World Radiation Center (PMOD-WRC), Davos, Switzerland
[3]Finnish Meteorological Institute, Helsinki, Finland
[4]Atmospheric Optics Group, Valladolid University, Valladolid, Spain
[5]Cimel Electronique, Paris, France

Correspondence: Emilio Cuevas (ecuevasa@aemet.es)

Abstract. A comprehensive comparison of more than 70 000 synchronous 1 min aerosol optical depth (AOD) data from three Global Atmosphere Watch precision-filter radiometers (GAW-PFR), traceable to the World AOD reference, and 15 Aerosol Robotic Network Cimel radiometers (AERONET-Cimel), calibrated individually with the Langley plot technique, was performed for four common or "near" wavelengths, 380, 440, 500 and 870 nm, in the period 2005–2015. The goal of this study is to assess whether, despite the marked technical differences between both networks (AERONET, GAW-PFR) and the number of instruments used, their long-term AOD data are comparable and consistent. The percentage of data meeting the World Meteorological Organization (WMO) traceability requirements (95 % of the AOD differences of an instrument compared to the WMO standards lie within specific limits) is > 92 % at 380 nm, > 95 % at 440 nm and 500 nm, and 98 % at 870 nm, with the results being quite similar for both AERONET version 2 (V2) and version 3 (V3). For the data outside these limits, the contribution of calibration and differences in the calculation of the optical depth contribution due to Rayleigh scattering and O_3 and NO_2 absorption have a negligible impact. For AOD > 0.1, a small but non-negligible percentage (~ 1.9 %) of the AOD data outside the WMO limits at 380 nm can be partly assigned to the impact of dust aerosol forward scattering on the AOD calculation due to the different field of view of the instruments. Due to this effect the GAW-PFR provides AOD values, which are ~ 3 % lower at 380 nm and ~ 2 % lower at 500 nm compared with AERONET-Cimel. The comparison of the Ångström exponent (AE) shows that under non-pristine conditions (AOD > 0.03 and AE < 1) the AE differences remain < 0.1. This long-term comparison shows an excellent traceability of AERONET-Cimel AOD with the World AOD reference at 440, 500 and 870 nm channels and a fairly good agreement at 380 nm, although AOD should be improved in the UV range.

1 Introduction

In recent decades there has been a growing interest in the role played by atmospheric aerosols in the radiation budget and the Earth's hydrological cycle, mainly through their physical and optical properties (IPCC, 2013). The most comprehensive and important parameter that accounts for the optical activity of aerosols in the atmospheric column is the aerosol optical depth (AOD) (WMO, 2003, 2005). This is also a key parameter used in atmospheric column aerosol modelling (e.g. Basart et al., 2012; Benedetti et al., 2018; Cuevas et al., 2015; Huneeus et al., 2016) and in satellite observations (e.g. Sayer et al., 2012, 2013;

Kahn and Gaitley, 2015; Amiridis et al., 2015). The second aerosol optical parameter in importance is the Ångström exponent (AE; Ångström, 1929) that accounts for the spectral dependency of the AOD. Since the AE is inversely related to the average size of the aerosol particles, it is a qualitative indicator of the atmospheric aerosol particle size, and therefore a useful parameter to assess the aerosol type (WMO, 2003). At present, two global ground-based radiometer networks provide aerosol optical properties of the atmospheric column using centralized data processing procedures based on their respective standard criteria and also centralized protocols for calibration and quality control, linking all network instruments. These are GAW-PFR (Global Atmosphere Watch precision-filter radiometer; http: //www.pmodwrc.ch/worcc/; last access: 5 September 2018) and AERONET-Cimel (AErosol RObotic NETwork Cimel Electronique radiometer; https://aeronet.gsfc.nasa.gov; last access: 1 September 2018) networks. AERONET is, in fact, a federation of ground-based remote-sensing aerosol networks established by NASA (National Aeronautics and Space Administration) and PHOTONS (PHOtométrie pour le Traitement Opérationnel de Normalisation Satellitaire, University of Lille, Service d'Observation de l'INSU, France; Goloub et al., 2007), complemented by other sub-networks, such as AEROCAN (Canadian sun photometry network; Bokoye et al., 2001), AeroSibnet (Siberian system for Aerosol monitoring; Sakerin et al., 2005), AeroSpan (Aerosol characterisation via sun photometry: Australia Network; Mitchell et al., 2017), CARSNET (China Aerosol Remote Sensing NETwork; Che et al., 2015) and RIMA (The Iberian network for aerosol measurements; Toledano et al., 2011). There are other radiometer networks that in recent years have incorporated centralized protocols for data evaluation and databases and performed regular intercomparisons with GAW-PFR and AERONET-Cimel. These include, for example, SKYNET (SKYradiometer NETwork) and its seven associated sub-networks, which use the Prede-POM sky radiometer to investigate aerosol–cloud–solar radiation interactions (e.g. Campanelli et al., 2004; Nakajima et al., 2007; Takamura and Nakajima, 2004).

The World Optical Depth Research Calibration Center (WORCC) was established in 1996 at the Physikalisch Meteorologisches Observatorium Davos World Radiation Center (PMOD-WRC). The GAW-PFR network (Wehrli, 2005) was initiated within PMOD-WRC for global and long-term atmospheric aerosol monitoring and accurate detection of trends. Aerosol data series measured at 12 core sites away from local and regional pollution sources that are representative of atmospheric background conditions in different climates and environments of the planet, in addition to another 20 associated stations, are included in this global network (Kazadzis et al., 2018a). For this reason, GAW-PFR uses the PFR, an accurate and reliable instrument regarding its absolute response stability over time that was designed for long-term AOD measurements (Wehrli, 2008a). The GAW-PFR was

specifically designed by WORCC for this goal following the technical specifications defined by the World Meteorological Organization (WMO, 2003, 2016). In 2006, the Commission for Instruments and Methods of Observation (CIMO) of the WMO (WMO, 2007) recommended that the WORCC at the PMOD-WRC should be designated as the primary WMO Reference Centre for AOD measurements (WMO, 2005).

The AERONET-Cimel network (Holben et al., 1998) was, in principle, designed to validate satellite products and to characterize the spatio-temporal distribution of atmospheric aerosols based on their optical properties. It is the largest surface-based global aerosol network, with more than 84 sites with measurement series longer than 10 years and more than 242 sites having datasets > 5 years. Cimel radiometer data, part of AERONET, are processed centrally and freely delivered in near real time by the NASA Goddard Space Flight Center. Both networks, although designed to meet different objectives, are now global benchmarks for the study and characterization of aerosol optical properties worldwide and for the evaluation of aerosol observations made on board satellites and simulations made using models. Multiple studies have proliferated in recent years to obtain aerosol climatology and to determine AOD trends in different parts of the world (e.g. Nyeki et al., 2012; Klingmüller et al., 2016; Chedin et al., 2018). However, these networks use radiometers with significant technical differences. Moreover, calibration methodologies, AOD calculation algorithms and data evaluation methods are also relatively different between the two networks. Consequently, the objective of this study is to assess whether, despite the marked differences between both networks, including the different day-to-day maintenance and operation procedures of the respective instruments during the study period, the long-term AOD data provided by the two networks are comparable and consistent.

The WMO has defined the GAW-PFR Triad (three Master PFR instruments) as the worldwide reference for AOD measurements (WMO, 2005). Based on this concept, an instrument provides traceable measurements of AOD to this WMO reference when this instrument can demonstrate an unbroken chain of calibrations between itself and the GAW-PFR Triad with AOD measurements within specified limits of the GAW-PFR reference. This can either be achieved by a direct comparison to the GAW-PFR Triad (Kazadzis et al., 2018a) or by using a portable transfer standard radiometer as presented in this study. Several comparisons between AERONET-Cimel, GAW-PFR and other radiometers have been carried out in different places (Barreto et al., 2016; Kazadzis et al., 2014, 2018b; Kim et al., 2008; McArthur et al., 2003; Mitchell and Forgan, 2003; Nyeki et al., 2015; Schmid et al., 1999; Toledano et al., 2012). However, these comparisons have been performed during field intercomparison campaigns or during relatively short periods of time, thus they are not representative of a large variety of atmospheric conditions. In addition, the type of instrument maintenance and the number and qualifications of staff serving them during campaigns is

generally of a higher quality compared to that of the instrument daily operation in unattended mode. This might cause an improvement in the instrument performance during intensive campaigns compared to the operational mode.

The growing interest in the analysis of long-term AOD and AE data series for climatological purposes requires an assessment of their quality assurance and long-term intercomparability. This is the first study to analyse the long-term traceability of AERONET-Cimel with respect to GAW-PFR and therefore to assess the validity of the long AOD and AE AERONET-Cimel data series for climatological and climate change studies under specific quality control requirements.

GAW-PFR has a comprehensive calibration system (Kazadzis et al., 2018a; Schmid and Wehrli, 1995) that is transferred by a worldwide suite of reference instruments. AERONET-Cimel does not have a WMO-CIMO linked reference and, as described by Holben et al. (1998), Eck et al. (1999) and Toledano et al. (2018), is based on maintaining reference AERONET radiometers based on the Langley calibration technique at Izaña, Spain, and Mauna Loa, USA. Calibration of all other instruments is based on raw voltage ratio comparisons with reference instruments at dedicated sites (Carpentras, France; Washington D.C., USA; Valladolid, Spain). There are few places in the world where synchronous observations of these two networks are available for long time periods and variable AOD conditions. The Izaña Observatory (IZO; Tenerife, Canary Islands) is one of them. The GAW-PFR measurements started at Izaña Observatory in 2001 (Wehrli, 2005), while AERONET-Cimel started in 2003 (Goloub et al., 2007). Since 2005, synchronous measurements (1 min values) that have been evaluated following the calibration procedures of each of the networks are available.

In addition, the Izaña Observatory is one of the two places in the world (the other is Mauna Loa, Hawaii, USA) where sun calibrations are performed using the Langley plot technique for both AERONET-Cimel and GAW-PFR reference instruments (Toledano et al., 2018) because of stable and very low AOD conditions during many days each year. Consequently, the instruments compared at the Izaña Observatory have been calibrated under the same environmental conditions, and therefore AOD differences can be directly linked with calibration principles, AOD post-processing and other instrumental differences. In this work, we analyse and evaluate the comparison of 11 years (2005–2015) of 1 min synchronous observations of AOD with AERONET-Cimel and GAW-PFR in four common or "near" wavelengths, assessing the results and explaining the possible causes of these differences. Some preliminary technical details on the traceability between GAW-PFR and AERONET-Cimel were reported in a technical report by Romero-Campos et al. (2017).

In Sect. 2 the facility in which this long-term comparison has been carried out is described. The technical characteristics of the AERONET-Cimel and GAW-PFR instruments are shown in Sect. 3, with special emphasis on the technical and methodological differences of both networks. Section 4 describes the methodology followed in this intercomparison based on the concept of WMO-GAW traceability. Results are given in Sect. 5. A summary and conclusions are provided in Sect. 6. The Supplement contains case analyses of inaccurate calibration and cloud contamination, some additional results of the comparison between PFR and Cimel with AERONET version 3 (V3), complementary information of the very short natural AOD variability, and the simulations performed with the Monte Carlo model to evaluate the impact of dust forward-scattering radiation on AOD determination.

2 Site description

Izaña Observatory (28.3° N, 16.5° W; 2373 m a.s.l.) is located in Tenerife (Canary Islands, Spain) and is managed by the Izaña Atmospheric Research Center (IARC), which is part of the State Meteorological Agency of Spain (AEMET). It is a suitable place for long-term studies of aerosol optical properties under contrasting atmospheric and meteorological conditions. This is because IZO is located in the free troposphere (FT) above the temperature inversion caused by the trade wind regime in lower levels and general subsidence associated with the branch of the decay of Hadley's cell aloft (Carrillo et al., 2016). This meteorological feature favours, during most of the year, the presence of pristine skies and clean air, representative of atmospheric background conditions (Cuevas et al., 2013; Rodríguez et al., 2009). On the other hand, its proximity to the African continent makes it a privileged site for observing and characterizing the Saharan Air Layer (SAL), which normally presents a high burden of desert mineral dust, especially during the summer months (Basart et al., 2009; Cuevas et al., 2015; Rodríguez et al., 2011). At that time of the year, the SAL impacts the subtropical free troposphere over the North Atlantic with large interannual (Rodríguez et al., 2015) and sharp intraseasonal (Cuevas et al., 2017a) variability. The contrasting atmospheric conditions that occur at IZO allow the comparison of the two networks, which can be performed under a wide range of AOD values: mostly for pristine conditions (AOD ≤ 0.03) but also for relatively high turbidity (AOD > 0.6) linked with dust-aerosol-related intrusions. In addition, the location offers the possibility of observing rapid changes in AOD, going from pristine conditions to dusty skies and vice versa in a matter of a few hours, especially in the summer period. The periodical presence of a dust-laden SAL allows us to evaluate the impact that the dust forward scattering into the field of view has on AOD retrieval. All this defines IZO as an excellent atmospheric aerosol natural laboratory to compare the performance of different radiometers measuring AOD. One of the first international AOD intercomparison campaigns was carried out at IZO in April 1984 (WMO, 1986), promoted and coordinated by PMOD-WRC.

The privileged conditions of pristine skies that characterize IZO during many days of the year have allowed this observatory to become a calibration site for the GAW-PFR and AERONET-Cimel networks since 2001 and 2003, respectively, where the extraterrestrial constants are determined with direct sun observations using the Langley plot technique (Toledano et al., 2018). Note that the extraterrestrial constant (calibration constant) is the signal the instrument would read outside the atmosphere at a normalized Earth–sun distance. In addition, since July 2014, IZO has also been designated by the WMO as a CIMO (WMO, 2014) test bed for aerosols and water vapour remote-sensing instruments. IZO is a station of the Baseline Surface Radiation Network (BSRN) (Driemel et al., 2018; García et al., 2019). Details of IZO facilities, measurement programmes and main research activities can be found in Cuevas et al. (2017b).

3 GAW-PFR and AERONET-Cimel radiometers

The two types of radiometers intercompared in this study are Cimel CE318-N (Holben et al., 1998), hereinafter referred to as Cimel, the standard instrument of AERONET until the recent appearance of CE318-T (Barreto et al., 2016), and the PFR (Wehrli, 2005), the standard instrument of the GAW-PFR network. The main features of these two radiometers are described in Table 1. The Cimel (Holben et al., 1994, 1998) is a radiometer equipped with a two-axis robot that performs two types of basic radiation measurements: direct solar irradiance and sky (radiance) observations, thanks to an automatic pointing robot that executes the observation sequences that have been scheduled. The robot performs automatic pointing to the sun by stepping azimuth and zenith motors using ephemeris based on time, latitude and longitude. Additionally, a four-quadrant detector is used to improve the sun tracking before each scheduled measurement sequence. This sensor guides the robot to the point where the intensity of the signal channel is at a maximum. Diffuse-sky measurements are also performed by Cimel to infer aerosol optical and microphysical properties. Two different routines are executed: almucantar (varying the azimuth angle keeping constant the zenith angle) and principal plane (varying the zenith angle keeping constant the azimuth angle). The ability of Cimel to perform both direct and diffuse-sky measurements makes it necessary to use a specific robot rather than a simple sun tracker. The field-of-view angle (FOV) of the instrument is 1.29° (hereafter ∼ 1.3°) (Torres et al., 2013). The wavelengths in which the measurements are sequentially made by a single detector depend on the interference filters that each version of the radiometer has installed in the filter wheel, which is located inside the sensor head and which is moved by a stepper motor. The Cimel versions used in this study have at least eight interference filters centred at 340, 380, 440, 500, 675, 870, 940, and 1020 nm and a 10 nm full-width-at-half-maximum (FWHM) bandwidth, except for

340 and 380 nm which have 2 and 4 nm FWHM, respectively. Solar irradiance is measured with a Silicon detector in these channels. The possible deterioration of the interference filters is reduced since they are only exposed to the sun during three consecutive 1 s direct sun measurements per channel, this cycle being scheduled every ∼ 15 min. The rest of the time the Cimel is taking sky radiance measurements or at rest position looking downwards.

The PFR (Wehrli, 2000, 2005, 2008a, b) is designed for continuous and automated operation under a broad range of weather conditions. It accurately measures direct solar radiation transmitted in four independent narrow wavelength channels centred at 368, 412, 500 and 862 nm, with a 5 nm FWHM bandwidth. The FOV of the instrument is 2.5° and the slope angle is 0.7°. Dielectric interference filters manufactured by the ion-assisted deposition technique are used to assure significantly larger stability in comparison to the one manufactured by classic soft coatings. The PFR was designed for long-term stable measurements; therefore, the instrument is hermetically sealed with an internal atmosphere that is slightly pressurized (2000 hPa) with dry nitrogen and is stabilized in temperature with a Peltier-type thermostatic system maintaining the temperature of the detector head at 20 °C ± 0.5 °C. This system makes corrections of the sensitivity for temperature unnecessary and also prevents accelerated ageing of filters, ensuring the high stability of the PFR. The PFR is mounted on a sun tracker, which is always pointing at the sun without any active optimization. The detectors are only exposed for short time periods, since an automated shutter opens every minute for 10 s for sun measurements, minimizing degradation related to the filter exposure.

The expected uncertainty of AOD in the four channels of the PFR radiometer is from 0.004 (862 nm) up to 0.01 (368 nm) (Wehrli, 2000). For the Cimel radiometer, the expected uncertainty of the level 2 AOD product is between 0.002 and 0.009 for reference instruments, larger for shorter wavelengths, between 0.01 and 0.02 for field instruments, and larger in the UV under the conditions of clear skies (Eck et al., 1999; Barreto et al., 2016). It should be taken into account that, in general, in the UV range the AOD uncertainty is higher (Carlund et al., 2017).

In relation to the calibration of both networks, GAW and AERONET, they use measurements at high mountain stations with very stable and low AOD over 1 d in which consecutive measurements can be performed over a wide range of optical air mass (approximately between 2 and 5) in the shortest possible time, in order to calibrate reference instruments using the Langley plot technique. In the case of AERONET-Cimel these calibrations are subsequently transferred to the field instruments of the network in other sites through regular intercomparison campaigns. In the case of the GAW-PFR, the calibration system is more complex in order to ensure traceability with the WORCC world reference. The maintenance of the AOD standard by the WORCC laboratory is described in Kazadzis et al. (2018b). It consists of

a triad of instruments that measure continuously and three additional standard portable transfer radiometers located at Mauna Loa (one instrument) and Izaña (two instruments) observatories. Every 6 months, one of the portable transfer standard radiometers visits the reference triad based at PMOD-WRC (Davos) and compares the calibration constants defined by the 6-month Langley calibrations in the two high mountain stations (Table 1 of Kazadzis et al., 2018b) with the one defined by the triad. The comparison is based on the signals (voltages) and not on AOD values. The differences between the Izaña GAW-PFR radiometers and the reference triad have been always lower than 0.5 %, being within the uncertainty of the Langley method, plus the small possible instrument degradations that can be detected in a 6–12-month period. Such degradations are quite small and are accounted for in the calibration analysis since extraterrestrial constants are linearly interpolated between two triad visits for every 6-month period. Additionally, the Izaña GAW-PFR "field" radiometers are calibrated on a routine basis using the Langley plot technique for double-checking quality assurance. Therefore, these radiometers cannot be considered simple field instruments but as regularly calibrated radiometers with assured traceability with the WORCC triad reference.

IZO is one of the two sites of Langley plot calibration of both networks, which represents an advantage when comparing the two instruments, eliminating, to a large extent, errors caused by the calibration transfer. However, there are differences between the calibration methodologies used by both networks. AERONET obtains the calibration by means of the average of a few extraterrestrial constants (V_0) obtained from Langleys and performed over a relatively short time (the time needed to collect data from at least 10 morning Langley plots). However, PFR-related Langleys are calculated by temporal linear fit to a larger number of extraterrestrial constants, V_0, obtained from Langley plots performed over 6 months (Wehrli, 2000; Kazadzis et al., 2018a). Details of requirements for performing Langley calibrations of reference instruments by GAW-PFR and AERONET and their uncertainties are analysed in detail by Toledano et al. (2018).

4 Data and methodology used in this study

The AOD at each wavelength is obtained from the Beer–Bouguer–Lambert law (Thomason et al., 1982; WMO, 2003) for radiometers collecting spectral direct sun measurements:

$$I(\lambda) = I_0(\lambda) \exp(-\tau m), \tag{1}$$

where $I(\lambda)$ is the direct sun signal at ground level at wavelength λ, $I_0(\lambda)$ is the extraterrestrial signal of the instrument corrected by the Earth–sun distance and m is the optical air mass in the measurement path (Kasten and Young, 1989). A detailed description of how AOD is obtained and the determination of extraterrestrial constants by GAW-PFR and AERONET is provided by Holben et al. (1994), Holben et al. (1998), Holben et al. (2001), Toledano et al. (2018), Wehrli (2000) and Wehrli (2008b).

4.1 GAW-PFR and AERONET-Cimel data

GAW-PFR provides AOD values every 1 min as an average of 10 sequential measurements with a total duration of less than 1 s (20 ms for each channel), then dark current is measured, going into sleep mode until the next minute. AERONET-Cimel takes a sequence of three separate measurements (1 s per filter) in 1 min interval (each one every 30 s). This sequence of measurements is called "triplet" and it is performed every ∼ 15 min for air masses lower than 2 and with higher frequency for lower solar elevations. Therefore, AERONET-Cimel provides AOD values for each triplet at least every ∼ 15 min. Note that AERONET-Cimel performs AOD measurements interspersed with sky radiance measurements, whose duration varies throughout the day, and therefore the AOD measurements are not necessarily provided at full minutes. We consider the 1 min data as synchronous when GAW-PFR and AERONET-Cimel AOD data were obtained with a difference of ∼ 30 s.

GAW-PFR and AERONET-Cimel instruments use the same time reference. The synchronization between the PC and GAW-PFR data logger was performed every 12 h since 2005 and improved to 6 h after 2013 using network time protocol (NTP) servers via the internet. From 2005 to 2012 the time of the AERONET-Cimel reference instruments was checked manually once a day using a handheld GPS. From 2012 onwards, the time was adjusted automatically three times a day using the ASTWIN Cimel software. In turn, the PC time is adjusted through the AEMET internal time server every 15 min. The AOD comparison has been performed using 1 min synchronous data from the four closest channels of both instruments in the period 2005–2015 (more than 70 000 data pairs in each channel). Thus, in the case of GAW-PFR, the four available channels of 368, 412, 500 and 862 nm were analysed, while in the case of AERONET-Cimel only the 380, 440, 500 and 870 nm channels were considered (Table 1). For the 500 nm channel, the nominal wavelengths of the two networks differ by a maximum of 1.8 nm. However, the nominal wavelengths in the rest of the compared channels present higher differences. Therefore, the AOD values of the original GAW-PFR 368, 412 and 862 nm channels have been interpolated or extrapolated to the corresponding AERONET-Cimel channels (380, 440 and 870 nm), using the Ångström power law and the GAW-PFR AE calculated from the four PFR AOD measurements.

Synchronous AE data provided by both instruments have also been compared (see Sect. 5.5). GAW-PFR determines AE using all four PFR wavelengths (Nyeki et al., 2015), while AERONET-Cimel uses different wavelength ranges (340–440, 380–500, 440–675, 440–870 and 500–870 nm) (Eck et al., 1999). As a consequence, we have calculated

a new AE for the Cimel radiometer using the four channel equivalent to those of the PFR.

In this study we have used the two versions of the AERONET database. Version 2 (V2) has been used so far in many scientific publications in high-impact journals and version 3 (V3) has been released just recently (Giles et al., 2019). In Sect. 5.1, a comparison of V2 and V3 is presented. A total of 3 GAW-PFR and 15 AERONET-Cimel instruments have been used in this intercomparison study covering the period 2005–2015. Their corresponding reference numbers are shown in Table 2.

4.2　Cloud filtering

The data matching in our comparison analysis was performed with synchronous 1 min AOD values of both networks labelled with quality control (QC) flags that guarantee proven quality data not affected by the presence of clouds. In the case of the AERONET-Cimel network, the selected AOD data are level 2 data from both V2 and V3 AERONET databases, which have been cloud filtered by the Smirnov algorithm (Smirnov et al., 2000), based on the triplet method with a second-order temporal derivative constraint (McArthur et al., 2003), and visually screened in V2. The cloud screening in AERONET V3 has been completely automated and notably improved, especially by refining the triplet variability and cirrus cloud detection and removal (Giles et al., 2019). These two cloud screening methods are able to detect rapid changes in the atmosphere and remove those measurements in which AOD variability within the triplet is higher than the following criteria:

- AOD triplet variability > MAX { 0.02 or 0.03 × AOD } at all wavelengths (V2)

- AOD triplet variability > MAX { 0.01 or 0.015 × AOD } at 675, 870 and 1020 nm simultaneously (V3)

The selection of these thresholds ensures the triplet average does not exceed 0.02 (V2) or 0.01 (V3) within 1 min in the case of low AOD conditions.

GAW-PFR cloud screening algorithms also use the Smirnov triplet measurement and the second-order derivative check but add a test for optically thick clouds with $AOD_{500\,nm} > 2$ (Kazadzis et al., 2018b). In the case of the GAW-PFR network (Wehrli, 2008a) the flags take the value 0 for cloudless conditions, no wavelength crossings and sun pointing within certain limits. More details are provided in Kazadzis et al. (2018a) for all of the selected records.

4.3　WMO traceability criteria

The criterion for traceability used in this study follows the recommendation of the WMO (WMO, 2005), which states that 95 % of the AOD measurements fall within the specified acceptance limits, taking the PFR as a reference:

$$U_{95} = \pm(0.005 + 0.010/m), \tag{2}$$

where m is the optical air mass. Note that the U_{95} range is larger for smaller optical air mass. The acceptance limits proposed by WMO take into account, on the one hand, the uncertainty inherent in the calculations of the AOD and, on the other hand, the uncertainty associated with the calibration of the instrument. The latter, for the case of instruments with finite field-of-view direct transmissions, such as the PFR and the Cimel, is dominated by the influence of the top-of-the-atmosphere signal determined by Langley plot measurements, divided by the optical air mass. The first term of Eq. (2) (0.005) represents the maximum tolerance for the uncertainty due to the atmospheric parameters used for the AOD calculation (additional atmospheric trace gas corrections and Rayleigh scattering). The second term describes the calibration-related relative uncertainties. The WMO recommends an upper limit for the calibration uncertainty of 1 %.

4.4　Modelling the impact of near-forward scattering on the AOD measured by the PFR and Cimel radiometers

In order to study the impact of near-forward scattering on the irradiance measured by the PFR and Cimel instruments, a forward Monte Carlo model (Barker, 1992, 1996; Räisänen et al., 2003) was employed. For the present work, the model was updated to account for the finite width of the solar disk (Räisänen and Lindfors, 2019). The starting point of each photon was selected randomly within the solar disk, assuming a disk half-width of 0.267° and the impact of limb darkening on the intensity distribution was included following Böhm-Vitense (1989). Some diagnostics were also added to keep track of the distribution of downwelling photons at the surface with respect to the angular distance from the centre of the sun. Gaseous absorption was accounted for following Freidenreich and Ramaswamy (1999), while the Rayleigh scattering optical depth was computed using Bodhaine et al. (1999).

5　Results

5.1　Comparison of long-term AERONET V2 and V3 datasets at Izaña site

Since V3 has been released recently (Giles et al., 2019), we present a comparison between V2 and V3 for the Cimel channels 380, 440, 500 and 870 nm for the period 2005–2015. The results indicate that for the Izaña site the agreement and consistency between the two AERONET versions is very high for the four channels ($R^2 > 0.999$), in full agreement with the results of the V2–V3 comparison reported by Giles et al. (2019). It follows that the results of the AOD comparison between GAW-PFR and the two versions of AERONET are very similar, as shown throughout this work. A detailed description of AERONET V3 and its improvements with respect to V2 is given in Giles et al. (2019). As such, improve-

Table 1. Main features of the GAW-PFR (PFR; Wehrli, 2000, 2005, 2008a, b) and AERONET-Cimel (Holben et al., 1994, 1998; Torres et al., 2013) radiometers used in this study.

	GAW-PFR	AERONET-Cimel
Type of instrument	Standard version	Standard version Reference instrument
Type of observation	Automatic continuous direct sun irradiance	Automatic sun–sky tracking
Available standard channels	368, 412, 500, 862 nm	340, 380, 440, 500, 675 nm, 870, 1020, 1640 nm
FWHM	5 nm	2 nm (340 nm), 4 nm (380 nm), 10 nm (VIS-NIR), 25 nm (1640 nm)
AOD uncertainty	±0.01	0.002–0.009, spectrally dependent, with higher errors in the UV (reference instruments) (Eck et al., 1999)
FOV (FWHM)	2.5° (1.2° plateau, 0.7° slope)	1.3° (slope angle unknown)
Sun tracker	Any sun tracker with a resolution of at least 0.08°	Robot specifically designed by CIMEL and controlled in conjunction with the radiometer
Temperature control and correction	Temperature controlled 20 °C ± 0.5 °C	Temperature correction to 1020 nm is applied in V2. Corrections from filter-specific temperature characterization in V3 for VIS and NIR spectral bands (Giles et al., 2019)
Power	Grid	Solar panels and grids
Data transmission	Local PC and FTP	Local PC and FTP Satellite transmission
Calibration	Comparison with reference triad. Additional in situ long-term Langleys	At least 10 good-quality morning Langley plots

Table 2. GAW-PFR and AERONET-Cimel instrument numbers used in this study in the period 2005–2015. Data from reference Cimel no. 398 were not upgraded to level 2 in V3 during the period 12 July–15 September 2008.

Instruments used in this study	Period 2005–2009	Period 2010–2015
GAW-PFR	2 instruments: no. 6, no. 25	2 instruments: no. 6, no. 21
AERONET-Cimel	13 instruments: no. 25, no. 44, no. 45, no. 79, no. 117, no. 140 no. 244, no. 245, no. 380, no. 382, no. 383, no. 398, no. 421	5 instruments: no. 244, no. 347, no. 380 no. 421, no. 548

ments depend on aerosol type, according to the changes introduced in V3, high mountain sites such as Izaña, characterized by low background AOD values or, alternatively, by the presence of dust (no pollution or biomass burning aerosols), show that the AOD differences between V2 and V3 are expected to be minimal, as is confirmed in this study (Fig. 1).

However, it should be noted that AERONET V3 does not restrict the calculation of AOD to optical air masses lower than 5.0 (Giles et al., 2019), as V2 does. This results in an increase in the number of solar measurements occurring in the early morning and the late evening. Consequently, the GAW-PFR comparisons with AERONET V3 consisted of ∼

9000 more data pairs than the GAW-PFR comparison with V2 (see Supplement S1).

5.2 AERONET-Cimel AOD comparison with GAW-PFR data

The comparison with GAW-PFR AOD shows that the AOD from AERONET-Cimel radiometers meet the WMO traceability criteria ("traceable AOD data" from now on) at the 440, 500 and 870 nm channels. The lowest agreement is found in the UV channel (380 nm), with 92.7 % of the data, and the highest in the infrared channel (870 nm), with 98.0 %
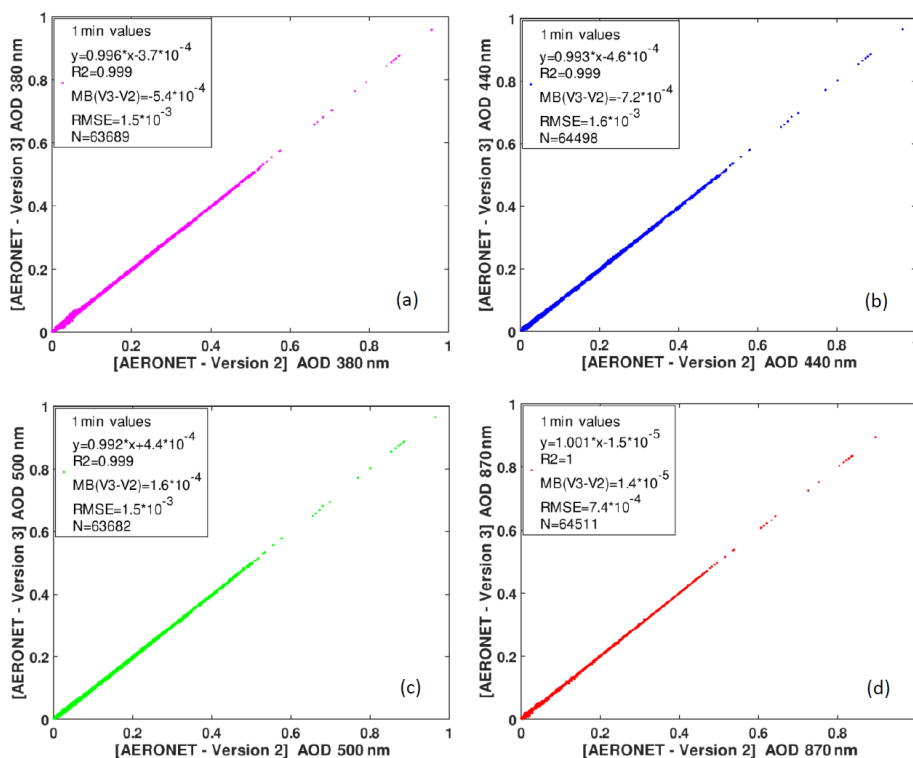
Figure 1. AERONET version 3 (V3) versus version 2 (V2) AOD 1 min data scatterplot at Izaña Observatory for the period 2005–2015: **(a)** 380 nm, **(b)** 440 nm, **(c)** 500 nm and **(d)** 870 nm. The corresponding equations of the linear fits, the coefficients of determination (R^2), mean bias (MB), root-mean-square error (RMSE) and the number of data pairs (N) used are included in each legend.

for V2 (Fig. 2; Table 3), because this channel is less affected by trace gas absorption. Almost identical results are obtained for V3 (Supplement S1 and S2.1). However, in the first half of the comparison period (2005–2009) there were some mechanical problems in the solar tracker that the GAW-PFR was mounted on, which caused sporadic problems in sun pointing. This finding was confirmed with data from the four-quadrant silicon detector (Wehrli, 2008a) that showed diurnal variation in the PFR sensors position up to 0.3°. From 2010 onwards, the PFR was mounted on an upgraded solar tracker with higher performance and precision. This reduced problems in sun pointing, which were the main cause of most of the AOD discrepancies between PFR and Cimel, and therefore not attributable to the instruments themselves. In addition, since 2010, Cimel no. 244 has been in continuous operation (for most of the time) at the Izaña Observatory, greatly simplifying calibration procedures and the corresponding data evaluation and minimizing errors of calibration uncertainties introduced by the use of a high number of radiometers in the intercomparison. During the 2010–2015 period, the fraction of traceable AOD measurements of the total between the AERONET-Cimel radiometer and the GAW-PFR improves to 93.46 % in the 380 nm channel and this percentage rises to 99.07 % for the 870 nm channel. Despite the technical differences between both radiometers de-

Table 3. Percentage of AERONET-Cimel (V2 and V3) 1 min AOD data meeting the WMO criteria for the four interpolated GAW-PFR channels for the period 2005–2015.

Channel (nm)	V2 (%)	V3 (%)
380	92.7	92.3
440	95.7	95.2
500	95.8	95.7
870	98.0	97.8

scribed above and the different calibration protocols, cloud screening, and data processing algorithms, the data series of both instruments can be considered equivalent, except for 380 nm, according to the WMO traceability criteria defined previously (Eq. 2). This explains the excellent agreement in the long-term AOD climatology shown for GAW-PFR and AERONET-Cimel in Toledano et al. (2018).

We have compared the percentages of AERONET-Cimel AOD V2 data meeting the WMO criteria for the four interpolated GAW-PFR channels with those of AERONET V3 (Table 3). A more detailed statistical evaluation for different scenarios of aerosol loading (three ranges of AOD) and aerosol size (three ranges of AE) for each compared channel has been performed (see Table 4). We observe that the poor-
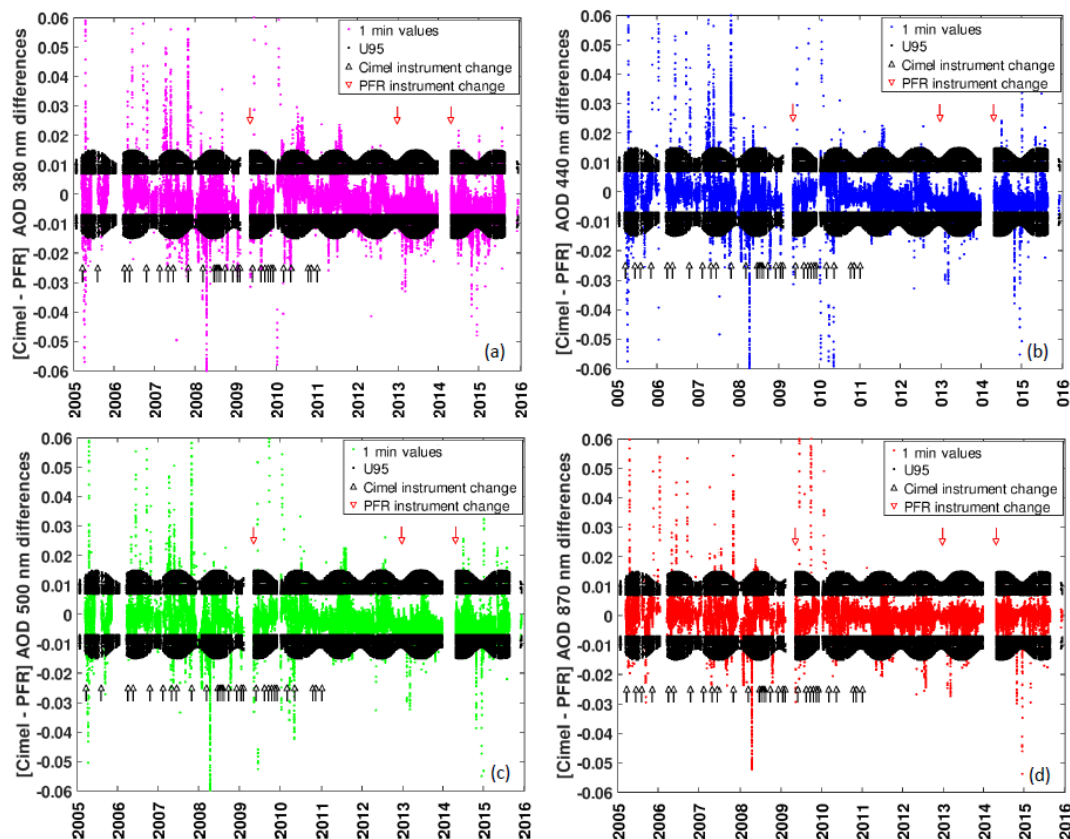
Figure 2. The 1 min AOD data differences between AERONET-Cimel (V2) and GAW-PFR for **(a)** 380 nm (70 838 data pairs), **(b)** 440 nm (71 645 data pairs), **(c)** 500 nm (70 833 data pairs) and **(d)** 870 nm (71 660 data pairs) for the period 2005–2015. Black dots correspond to the U_{95} limits. A small number of outliers are out of the ~ 0.06 AOD difference range. Black arrows indicate a change of reference AERONET-Cimel radiometer and red arrows indicate a change of the GAW-PFR instrument.

est agreement is obtained at the shorter wavelength channels (440 nm and especially 380 nm). Kazadzis et al. (2018b) also found a decrease in the percentage of AOD meeting the WMO criteria for 368 and 412 nm spectral bands during the Fourth WMO Filter Radiometer Comparison for aerosol optical depth measurements. As these authors pointed out, the shorter the wavelength, the poorer the agreement due to several reasons: AOD in the UV suffers from out-of-band leakage or at least different blocking of the filters, small differences in central wavelength or FWHM have a larger impact, the Rayleigh correction is more critical, and NO_2 absorptions are treated differently. Regarding the effect of the aerosol load and particle size on the AOD differences, our results confirm the decrease in agreement between the two instruments for very large particles is coincident with almost pure dust (AE ≤ 0.3) and high turbidity conditions (AOD > 0.1). However, it should be noted that the percentage of data pairs in these situations is relatively low (e.g. 6 % for AOD > 0.1 and 3.2 % for AE < 0.25 at 380 nm) with respect to the total data (Table 4). A similar result was reported by Kim et al. (2008), who attributed these discrepancies to the possible spatial and temporal variability of aerosols under larger op-

tical depths, in addition to the effect of the different FOV of both radiometers. In our case, and according to previous studies on AOD climatology at IZO (Barreto et al., 2014), the presence of high mineral dust burden when the station is within the SAL does not necessarily imply lower atmospheric stability conditions resulting in daily AOD means with greater standard deviation. For these reasons, we assumed that the different FOV of these instruments is the main cause of part of the AOD 1 min differences outside the U_{95} limits under high AOD conditions. This issue is specifically addressed in Sect. 5.3.

In general, the agreement obtained with the 1 min AOD data is slightly lower than that obtained during short campaigns, such as those reported by Barreto et al. (2016) at IZO (5566 data pairs), with agreement of > 99 % for AOD$_{870\,nm}$ and AOD$_{500\,nm}$. However, our results for AOD$_{500\,nm}$ (> 95 % of 70 833 data pairs) are significantly better than those observed by Kazadzis et al. (2014) (~ 48 % of 468 data pairs) covering a relatively narrow range of AOD. In addition, short-term campaigns usually cover a small range of AOD, and instruments are carefully and frequently supervised. On the contrary, during our intercomparison over a period of

Table 4. Percentage of AERONET-Cimel 1 min AOD data (V2) meeting the WMO criteria for the four compared channels and different AOD and AE scenarios for the period 2005–2015. The last row corresponds to the total percentages for the sub-period 2010–2015. AOD and AE traceability > 95 % are marked in bold. The number of data pairs is in brackets.

Percentage of data within WMO limits	380 nm	440 nm	500 nm	870 nm
AOD ≤ 0.05	94.4 (57 008)	**96.8 (59 130)**	**97.0 (58 572)**	**98.5 (60 191)**
0.05 < AOD ≤ 0.10	91.0 (4723)	93.1 (4850)	92.8 (4817)	94.2 (4908)
AOD > 0.10	75.0 (3938)	86.5 (4615)	85.1 (4466)	**95.9 (5118)**
AE ≤ 0.25	73.1 (2145)	82.3 (2417)	80.1 (2351)	**96.2 (2824)**
0.25 < AE ≤ 0.6	91.2 (5407)	**96.2 (5810)**	**96.0 (5691)**	**97.9 (5911)**
AE > 0.6	94.6 (55 114)	**96.9 (57 089)**	**97.0 (56 504)**	**98.7 (58 146)**
Total 2005–2015	92.7 (65 669)	**95.7 (68 595)**	**95.8 (67 855)**	**98.0 (70 217)**
Total 2010–2015	93.5 (41 977)	**97.4 (43 745)**	**97.2 (43 627)**	**99.1 (44 498)**

11 years, the operation of the instruments can be considered the normal operation of such a system. An additional interesting aspect of this study is that it is not a simple intercomparison exercise between two instruments but a comparison of a number of instruments that acted as reference instruments for the AERONET Europe network.

In the first period (2005–2009), a total of 13 Cimel radiometers were used, while in the second period (2010–2015) 5 Cimel radiometers were used, and for much of this period Cimel no. 244 was operating as the permanent AERONET reference instrument at IZO. Once the most important causes of non-traceability in the first period, which were associated with a poor pointing of GAW-PFR due to problems in the sun tracker, were discounted, we can conclude that there are no significant differences in the percentages of traceable data between the two periods. This means that the continuous change of reference Cimel instruments used in the 2005–2009 period did not have a significant impact on AOD data comparison differences. This provides proof of the consistency and homogeneity of the long AERONET-Cimel AOD data series and their comparability with the GAW-PFR AOD data series, regardless of the number of instruments used to generate these data series. In our study, with a number of comparison data pairs 1 or 2 orders of magnitude higher than those used in short campaigns, the results shown in Table 4 can be considered fairly good.

In addition to the traceability scores, we have introduced some basic skill scores corresponding to the AOD intercomparison between GAW-PFR and AERONET-Cimel for the period 2005–2015 (Table 5) to be in line with previous studies that have performed short-term comparisons between these two instruments. The definitions of the used skill scores can be found in Huijnen and Eskes (2012). The Pearson's correlation coefficient (r) values of the Cimel–PFR 1 min AOD data pairs are higher than 0.99 in all channels. Concerning mean bias (MB) and root-mean-square error (RMSE) associated with AOD differences, our results show quite similar skill scores to those found at Mauna Loa, USA, for $AOD_{500\,nm}$ (Kim et al., 2008), although the number of data pairs used at IZO ($\sim$ 71 000) is much higher and the AOD

range of our study is much larger than that of the comparison performed at Mauna Loa. Kim et al. (2008) summarize results of previous short-term intensive studies (McArthur et al., 2003; Mitchell and Forgan, 2003; Kim et al., 2005; Schmid et al., 1999) carried out at stations where the radiometers were calibrated by intercomparison with reference instruments. These results show MB values to be within 0.01 bias, 1 order of magnitude larger than at the Mauna Loa and Izaña Observatories, highlighting the importance of having well-calibrated instruments to carry out these type of comparisons. For the period 2010–2015 (not shown here), as expected, the RMSE and the Pearson's correlation improve slightly compared to the whole period 2005–2015.

In relation to the comparison between GAW-PFR and AERONET-Cimel V3, we have calculated the percentage of AERONET-Cimel 1 min AOD data (V3) meeting the WMO criteria for optical air mass > 5.0 for the period 2005–2015 (Supplement S2.2). The results are somewhat poorer than for optical air mass < 5.0, since the solar elevation is very low. Only for the 870 nm channel does 95 % of the data meet with the WMO criteria, although the percentages of data in the 440 and 500 nm channels are close to this value. This would be the main reason to find slightly poorer traceability results with all V3 data compared to those found with V2 for which the AOD data are limited to optical air mass < 5.0.

5.3 Non-traceability assessment

As presented in Table 3, data outside the WMO traceability criteria vary from 2 % for 870 nm up to 7.3 % for 380 nm. In this section, the different possible causes of non-traceability in AOD are evaluated and, if possible, quantitatively estimated. In order to assess the relevance and quantitative impact of these causes and estimate errors derived from a non-perfect AOD data synchronization, we first made an analysis on the natural variability of AOD in a very short time period (1 min) shown below.

Table 5. Basic skill scores from the AOD intercomparison between GAW-PFR and AERONET-Cimel V2 for the period 2005–2015. The skill score definitions are found in Huijnen and Eskes (2012).

Period	2005–2015			
Wavelengths (nm)	380	440	500	870
Mean bias (MB)	−0.0026	−0.0018	−0.0021	−0.0001
Modified normalized mean bias (MNMB)	−0.1301	−0.1046	−0.1474	0.0129
Fractional gross error (FGE)	0.1727	0.1546	0.1918	0.1837
Root-mean-square error (RMSE)	0.0081	0.0070	0.0064	0.0049
Pearson's correlation coefficient (r)	0.9910	0.9925	0.9939	0.9949
Number of data pairs	70 838	71 645	70 833	71 660

Table 6. Percentage of AOD data with variability within 1 min of less than 0.01 and 0.005, using AOD data from GAW-PFR (at 368 and 501 nm) and AERONET-Cimel (at 380 and 500 nm), respectively, for 2013. A total of ∼ 32 000 data pairs per channel have been used from GAW-PFR and 20 117 triplets (60 351 individual AOD measurements) from Cimel no. 244 have been used to calculate the AOD variability.

GAW-PFR		
Percentage of data with 1 min AOD variability (%)		
	368 nm	501 nm
< 0.01	99.8	99.91
< 0.005	99.21	99.35
AERONET-Cimel		
Percentage of data with 1 min AOD variability (%)		
	380 nm	500 nm
< 0.01	99.87	99.99
< 0.005	99.82	99.42

5.3.1 Short-term AOD variability

In order to determine the variability of AOD within 1 min, we have performed two independent analyses with AOD data from the PFR (at 368 and 501 nm) and Cimel (at 380 and 500 nm) channels during 1 year (2013). On the one hand, and taking into account that GAW-PFR provides AOD every minute, we have calculated all the AOD differences for each channel in the successive minutes. So we have the variation in AOD from 1 min to the next one during a whole year. On the other hand, for AERONET-Cimel, we have taken advantage of the triplets, since each triplet consists of three successive measurements made in 1 min. In this case, the strategy has been to calculate the standard deviation of the triplet AOD measurements during a whole year.

The results obtained of the AOD variability in 1 min from PFR data are very similar and consistent to those obtained

with Cimel. Less than ∼ 0.8 % of the AOD data show variability higher than 0.005 in all wavelength ranges. It should be noted that the possible instrumental noise is included in this variability, so that the actual natural AOD variability would be, in any case, lower than that expressed in Table 6. The percentage of data with 1 min AOD variability for all four GAW-PFR channels is given in Supplement S3.1.

We have also determined the percentage of 1 min AOD data from the Cimel triplets (from 2013), whose diurnal range of variation is $\mathrm{AOD_{max} - AOD_{min} > 0.015}$, for several AOD intervals. Note that this value is half of the WMO traceability interval when $m = 1$ (maximum possible interval) (see Eq. 2). The results shown in Supplement S3.2 indicate that the 1 min AOD variability is responsible for only 0.11 % (0.01 %) of 1 min Cimel AOD values outside the WMO limits in the [0–0.03] AOD range (pristine conditions) for 380 nm (500 nm). The AOD variability maximizes in the 0.1–1 AOD range causing 2.31 % and 1.69 % of the AOD data outside WMO limits for 380 and 500 nm, respectively. This last scenario corresponds, as expected, to changes of air masses, such as transitions from pristine to dusty conditions and vice versa, or to the sharp onset and disappearance of very sporadic biomass burning plumes. In any case, the AOD data with 1 min variability exceeding 0.02 (V2) or 0.01 (V3) are filtered by AERONET (see Sect. 4.2) and therefore are not included in the GAW-PFR and AERONET-Cimel comparison.

These results indicate that the natural AOD variability is very low, thus the non-ideal measurement synchronization cannot explain the percentages of non-traceable AOD cases shown in Tables 3 and 4.

5.3.2 Uncertainties of GAW-PFR channel interpolation to AERONET-Cimel channels

The interpolation of the CIMEL AODs to the PFR AOD wavelengths can be one of the sources of uncertainty in this comparison assessment. The greatest uncertainty arises in the extrapolation of the $\mathrm{AOD_{412\,nm}}$ of the PFR to the Cimel wavelength 440 nm. Using the Ångström formula we have calculated that for an uncertainty of ±0.5 in the AE the introduced uncertainty in the AOD extrapolation from 412 to

440 nm is ∼ 5 % (i.e. 0.005 for $AOD_{412\,nm} = 0.1$). The introduced uncertainty in AOD extrapolation is reduced to ∼ 2 % for an uncertainty of ±0.3 in AE. For all other AOD interpolations the errors are smaller.

5.3.3 Calibration-related errors

As described in Sect. 3, the calibration procedures of the AERONET-Cimel and GAW-PFR radiometers are different. While in the case of GAW-PFR frequent calibrations are established throughout the year and the calibration value is linearly interpolated in time, in AERONET-Cimel a constant calibration value is assumed in the intermediate period between two consecutive calibrations carried out on an annual basis. The typical calibration uncertainty for a single Langley plot is 0.7 %–0.9 % (at the 95 % confidence level) and it is reduced to 0.4 % in the case of IZO when averaging at least 10 Langley-derived extraterrestrial constants (which is the normal procedure) (Toledano et al., 2018). Regarding the GAW-PFR radiometers operated at IZO, a direct yearly comparison of the Langley-based V_0 with the reference triad at PMOD-WRC showed differences lower than 1 % for all channels for the 2005–2015 period.

An insufficiently accurate determination of the calibration constant results in a fictitious AOD diurnal evolution presenting a concave or convex characteristic curve due to the calibration error dependence on solar air mass. The largest error occurs in the middle part of the day (lower air masses), mainly on clean days with very low aerosol load (< 0.02 in 500 nm), as reported by Romero and Cuevas (2002) and Cachorro et al. (2004) and can be derived from Eq. (2). According to Cachorro et al. (2004, 2008), fictitious differences of up to 0.06 between the minimum and the maximum AOD can be recorded in a day with constant AOD as a result of a non-accurate calibration or non-cleaned instruments. However, these fictitious differences in AOD depend on the related calibration magnitude errors.

We have represented the AOD differences between GAW-PFR and AERONET-Cimel versus optical air mass for the four channels for pristine conditions ($AOD_{500\,nm} \leq 0.03$) for both V2 and V3 (see Supplement S4). It should be noted that although the few outliers are evenly distributed throughout the whole air mass range, they are not equally distributed with respect to the zero of the AOD difference, but there is a bias with positive large outliers (higher Cimel AOD), already reported by Nyeki et al. (2013), and small negative outliers for optical air mass lower than 2.

The total percentage of AOD traceable data pairs under pristine conditions ($AOD_{500\,nm} \leq 0.03$) is very high for all wavelengths (> 97.7 %) falling within the U_{95} limits (Table 7), except for 380 nm. There is no dependence on 1 min AOD differences with optical air mass for 440, 500 and 870 nm and a slight dependence for 380 nm (Table 7) with a higher percentage of AOD differences outside the U_{95} limits at lower optical air masses. For the extended range of optical air mass > 5 in V3, the AOD differences do not increase with optical air mass (Supplement S5). The lower traceability at 380 nm for low air masses is especially clear in V3, with 92.9 % of traceable data (see Supplement S5). This result is consistent with the fact that the highest uncertainty in the determination of the calibration constants is observed in the UV range and the lowest uncertainty in the near-infrared channel (Eck et al., 1999; Jarosławski et al., 2003; Toledano et al., 2018). This is attributable to an imperfect calibration or to very small changes in the filters' transmittance, which can only be detectable in extreme conditions: UV range, very low optical air mass and pristine conditions. According to Toledano et al. (2018), the greatest variance in the extraterrestrial constant in the UV channel could be due to a number of factors: (1) higher AOD variability at the shorter wavelengths, (2) filter blocking issues or (3) temperature effects affecting AERONET-Cimel instruments that have not been accounted for in the UV range.

The correct cause attribution of each outlier would require manual inspection and additional specific information on instrumental checking and maintenance information that is not always available. We have investigated in more detail the origin of the outliers and whether one of the two instruments predominantly caused them. Thus, we have calculated for the non-traceable AOD data the diurnal range of AOD variation (maximum value minus minimum value of AOD over 1 d) at 380 nm for each instrument under pristine conditions (Fig. 3), using Cimel $AOD_{500\,nm}$ daily mean < 0.03 to select the pristine days. According to this approach, the instrument that shows the highest daytime AOD range is the one that is responsible for the outlier. As the wavelength increases, both the number of outliers and the magnitude thereof decreases significantly (Supplement S6). Then, we identified those outliers with a diurnal AOD range higher than 25 % of the mean daily AOD value and investigated their possible causes. A total of 51 cases for GAW-PFR and 81 cases for AERONET Cimel V3 were obtained and analysed in detail, using auxiliary information, such as 1 min in situ meteorological data, 5 min all-sky images, 1 min BSRN data and satellite imagery (not shown here). We obtained the percentage of AOD outliers of GAW-PFR and AERONET Cimel (V3) for which a certain cause has been identified, such as calibration uncertainties, cloud screening algorithm failures, mixture of the two previous causes, poor sun pointing or poorly defined causes (electronic problems, humidity inside the lenses, filter dirtiness, obstruction of the lenses collimators, insects on the optics outside, etc.) (see Supplement S7).

From the analysis of these cases, under the conditions described above, it should be noted that ∼ 44 % of the cases with fictitious AOD diurnal cycles were due to small uncertainties in the calibration of AERONET-Cimel (V3), while for this same cause ∼8 % of cases were identified in GAW-PFR. Some examples of AOD non-traceability for both AERONET-Cimel and GAW-PFR in the ∼ 380 nm channel are shown in Supplement S8. The fictitious diurnal AOD cy-

Table 7. Percentage of 1 min AOD data (V2) meeting the WMO criteria for each wavelength for different optical air mass intervals under pristine conditions (AOD$_{500\,nm} \leq 0.03$) in the period 2005–2015. See Supplement S5 for equivalent results with V3.

Percentage of AOD differences within the U_{95} limits AOD$_{500\,nm} \leq 0.03$	Total	$1 \leq m < 2$	$2 \leq m < 3$	$3 \leq m < 4$	$4 \leq m < 5$
	(%)	(%)	(%)	(%)	(%)
380 nm	95.8	94.5	96.0	97.4	97.2
440 nm	97.9	97.9	97.7	98.2	97.7
500 nm	98.3	98.4	98.1	98.6	98.4
870 nm	99.2	99.4	99.3	99.2	98.6
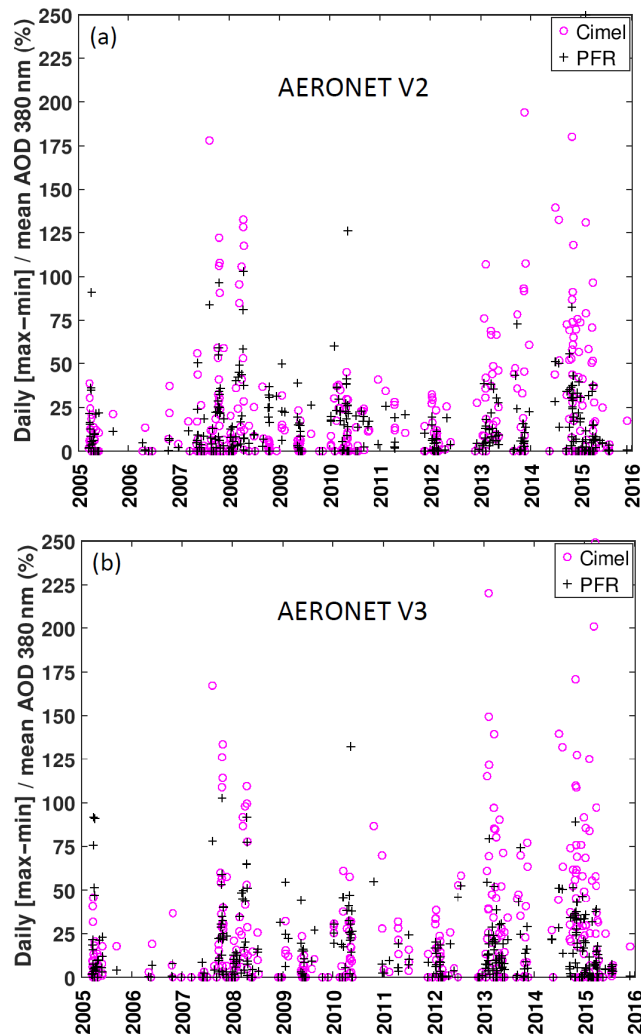
Figure 3. AOD diurnal range variation (maximum value minus minimum value of AOD in 1 d) at 380 nm corresponding to AOD outliers (non-traceable AOD) under pristine conditions (AOD$_{Cimel-500\,nm} \leq 0.03$) in the period 2005–2015 for AERONET V2 **(a)** and V3 **(b)**.

cle is mainly visible in the UV channels, as shown in the examples reported in Supplement S9, where the convex or concave diurnal AOD curvature symmetrical at noon provides a hint of calibration inaccuracies. Note that the fictitious diurnal AOD can be more easily identified under very low AOD conditions. We should emphasize that the rare finding of small calibration inaccuracies in a high mountain site with pristine skies and a stable atmosphere does not detract from the quality of any instrument as they often measure near or below the detection limit. Simply, these small inaccuracies are the result of limitations in the photometric measurement technique.

5.3.4 Differences in cloud screening and sun tracking

We have examined the effect that the presence of clouds might have on AOD differences and the percentage of cases outside the U_{95} limits. The impact of clouds on AOD differences only occurs when both GAW-PFR and AERONET-Cimel cloud screening algorithms fail to identify clouds in the direct sun path. In order to assess the impact that cloud conditions might cause on AOD traceability, we have used the concept of daily fractions of clear sky (FCS), which has been applied before to solar radiation data at IZO (García et al., 2014). FCS represents the percentage of observed sunshine hours in a day with respect to the maximum possible sunshine hours in that day. The higher the daily FCS, the higher the clear sky percentage we have on that day. The percentages of traceable and non-traceable AOD data versus FCS values grouped into five intervals are shown in Table 8. It should be emphasized that the number of cases linked with FCS between 0 % and 60 % are less than 2 % of the total cases. As the fraction of clear sky increases, the percentage of traceable AOD data significantly exceeds the number of non-traceable AOD data. The percentage of traceable data is especially large (> 90 %) when FCS > 80 % (almost clear skies).

This is the FCS range in which a significant percentage of days with cases presenting scattered clouds are recorded, which qualitatively confirms that V3 has introduced more efficient cloud screening than V2. However, the real impact of clouds on AOD traceability at IZO is very low due to its special characteristics as a high mountain station with very lit-
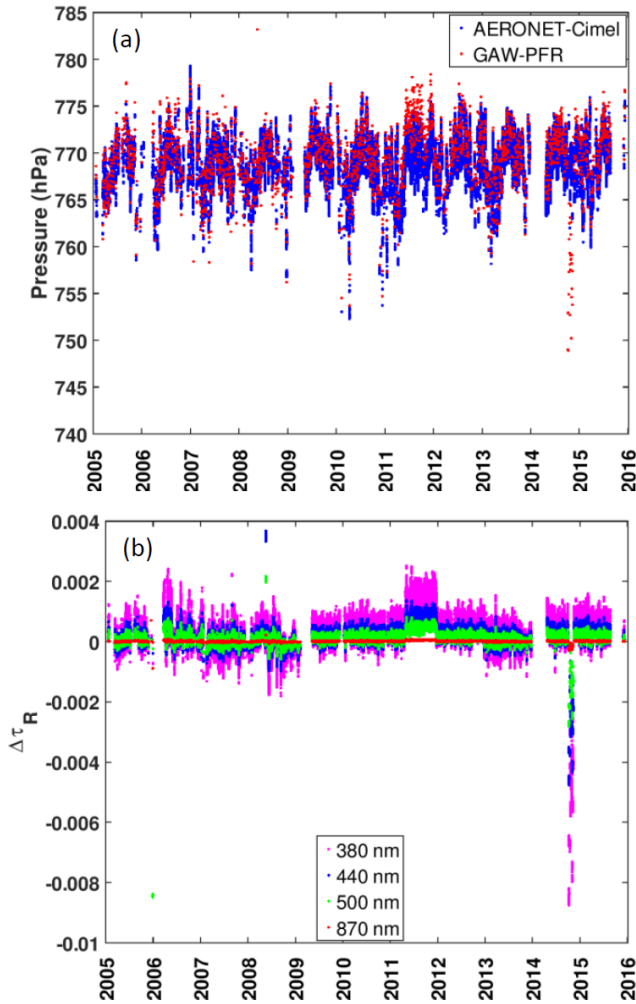
Figure 4. (a) The 1 min pressure data (hPa) from GAW-PFR and 6 h pressure data at Izaña Observatory from the National Centers for Environmental Prediction (NCEP) and the National Center for Atmospheric Research (NCAR) reanalysis for the case of AERONET-Cimel and **(b)** corresponding 1 min $\Delta\tau_R$ caused by pressure differences in the period 2005–2015.

tle cloudiness. Therefore, in practice, the possible impact of clouds on the non-traceability of AOD data pairs is insignificant at IZO. GAW-PFR and AERONET-Cimel cloud screening algorithms provide successful identification of clear direct sun conditions during cloudy skies (FCS < 40 %) for 99.75 % of the cases, excluding those with very thin clouds.

In the particular case of Izaña, there are two specific cloud scenarios in which cloud screening algorithms could fail, resulting in non-AOD traceability: (1) cirrus clouds (see Supplement S10) and (2) low clouds (stratocumulus), which sometimes exceed the observatory height level (see Supplement S11). As can be deduced from the analysis of these cloud cases, the impact of the different types of clouds on AOD retrieval is very complex and further specific investigations are required in order to understand the reasons be-

hind failures in the GAW-PFR and AERONET-Cimel cloud screening algorithms.

5.3.5 Rayleigh scattering, absorption by O_3 and NO_2 corrections

In this section, we evaluate the possible impact on the 1 min AOD data outside the U_{95} limits due to the different processing of each network regarding the correction by Rayleigh scattering and by the light absorption of column O_3 and NO_2. Although GAW-PFR and AERONET-Cimel use spectral channels with weak absorption by atmospheric gases, AOD can only be determined if optical depth contributions from those gases are well estimated and subtracted from the total optical depth (τ). GAW-PFR and AERONET-Cimel separate the contributions of the molecules (Rayleigh scattering, τ_R), aerosols (τ_a, in this study referred to as AOD) and absorbing gases, i.e. total column ozone (τ_{O_3}) and nitrogen dioxide (τ_{NO_2}), due to their different optical air masses at low solar elevation:

$$I(\lambda) = I_0(\lambda)\exp-(\tau_R m_R + \tau_a m_a + \tau_{O_3} m_{O_3} + \tau_{NO_2} m_{NO_2}). \tag{3}$$

Thus, AOD can be derived as follows:

$$\text{AOD} = \frac{1}{m_a}\left(\ln\frac{I_0(\lambda)}{I(\lambda)} - \tau_R m_R - \tau_{O_3} m_{O_3} - \tau_{NO_2} m_{NO_2}\right). \tag{4}$$

Rayleigh scattering

The Rayleigh-scattering contribution to total optical depth would be as follows:

$$\tau_R = \delta_R \frac{m_R}{m_a}, \tag{5}$$

where m_R is written, according to Kasten and Young (1989), as follows:

$$m_R = \frac{1}{\sin\theta + 0.50572(\theta + 6.07995)^{(-1.6364)}}, \tag{6}$$

and m_a, according to Kasten (1966), has the following expression:

$$m_a = \frac{1}{\sin\theta + 0.0548(\theta + 2.65)^{(-1.452)}}, \tag{7}$$

where θ is the sun elevation and δ_R can be expressed as follows (Bodhaine et al., 1999):

$$\delta_R(\lambda) = 0.00864\lambda^{-\left(3.916 + 0.074\lambda + \frac{0.050}{\lambda}\right)}\frac{P}{P_o}, \tag{8}$$

where $P_o = 1013.25$ hPa, λ is the wavelength in microns (μ) and P is the pressure in hPa at the measurement site. The depolarization factor recommended by (Young, 1980) is already included in Eq. (8). From Eq. (8), we can derive the

Table 8. Percentage of AOD data within the U_{95} limits for each channel and five daily fractions of clear sky (FCS) intervals. In brackets, the relative frequency of each FCS interval is given for AERONET V2 and V3, respectively. In bold are the percentages of V3 that are greater than those of V2.

	380 nm		440 nm		500 nm		870 nm	
	V2	V3	V2	V3	V2	V3	V2	V3
0 % ≤ FCS < 20 % (0.03 %) (0.04 %)	47.6	44.4	43.5	44.4	47.6	44.4	87.0	**92.6**
20 % ≤ FCS < 40 % (0.22 %) (0.22 %)	69.3	**76.6**	73.3	**82.2**	73.6	**80.8**	86.3	**94.1**
40 % ≤ FCS < 60 % (1.08 %) (1.09 %)	79.1	77.5	87.8	84.8	88.8	87.2	91.9	**92.0**
60 % ≤ FCS < 80 % (7.10 %) (7.17 %)	88.4	**89.6**	93.9	93.9	93.4	**94.4**	97.8	97.6
FCS ≥ 80 % (91.6 %) (91.5 %)	93.3	92.8	96.2	95.6	96.2	96.1	98.3	98.1

differences in τ_R contribution as follows ($\Delta\tau_R$):

$$\Delta\tau_R = \left(0.00864\lambda^{-\left(3.916+0.074\lambda+\frac{0.050}{\lambda}\right)}\frac{1}{1013.25}\frac{m_R}{m_a}\right)$$
$$(P_{\text{PFR}} - P_{\text{Cimel}}). \tag{9}$$

Accordingly, the main τ_R from GAW-PFR and AERONET-Cimel can arise from the different way the two instruments obtain atmospheric pressure (P_{PFR} and P_{Cimel}, respectively). While AERONET-Cimel obtains the site station pressure from the National Centers for Environmental Prediction (NCEP) and the National Center for Atmospheric Research (NCAR) reanalysis at standard levels, GAW-PFR has a solid-state pressure transducer in the control box to read barometric pressure simultaneously with each PFR measurement. As Giles et al. (2019) have stated, the expected error in the station pressure P_{Cimel} is generally < 2 hPa, provided the elevation of the station is well known and the weather conditions are stable. In order to assess this possible difference, we have compared the 1 min synchronous pressure data of both instruments and the corresponding 1 min $\Delta\tau_R$ from Eq. (9). Note that, in practice, this comparison is performed at 6 h intervals since the NCEP–NCAR reanalysis data are available routinely with this temporal resolution (Kalnay et al., 1996). The results are depicted in Fig. 4.

The results indicate that most of the 1 min pressure differences are within ±5 hPa (Fig. 4a), resulting in 1 min $\Delta\tau_R$ data within ± 0.001. However, when pressure differences are significantly higher, such as those registered at the end of 2014 (> 30 hPa) (Fig. 4a), $\Delta\tau_R$ increases significantly (∼ 0.01) (Fig. 4b). However, it should be noted that only 99 AOD data pairs have been registered for which the pressure difference between PFR and Cimel is greater than 20 hPa at 870 and 440 nm and one AOD data pair at 500 and 380 nm channels. Taking into account that the accuracy of the new barometers built into new radiometers is ∼ 3 hPa, only dramatic barometer malfunctioning could cause $\tau_R > 0.01$. As

stated by Kazadzis et al. (2018b), the use of erroneous pressure values can lead to wavelength-dependent AOD errors and to large errors in AE. However, these flagrant barometer malfunctions are quickly detected and easily corrected if there are other pressure measurements at the station, as is the case at Izaña.

Differences in O$_3$ absorption

The O$_3$ optical depth is determined with the following expression:

$$\tau_{O_3}(\lambda) = \sigma_{O_3}(\lambda)\frac{O_3}{1000}\frac{m_{O_3}}{m_a}, \tag{10}$$

where O$_3$ is expressed in Dobson units (DU) and the absorption coefficients ($\sigma_{O_3}(\lambda)$) take the following values (Gueymard, 1995): $0.0026\,\text{cm}^{-1}$ (440 nm), $0.03150\,\text{cm}^{-1}$ (500 nm) and $0.00133\,\text{cm}^{-1}$ (870 nm). The ozone absorption is at a maximum in the 500 nm channel and zero in the 380 nm channel. GAW-PFR uses for m_{O_3} the following expression (Komhyr, 1980):

$$m_{O_3} = \frac{R+h}{\sqrt{(R+h)^2 - (R+r)^2(\cos\theta)^2}}, \tag{11}$$

where $R = 6370$ km is the mean radius of the Earth, $r = 2.370$ km is the altitude of the station, $h = 22$ km is the estimated height of the ozone layer and θ is the solar elevation. However, AERONET-Cimel uses an updated expression (Komhyr et al., 1989) in which h is not fixed and takes a value in function of the latitude and the absorption coefficients are obtained for each particular filter using the spectral response provided by the manufacturer.

For most of the period covered in this study, measured total ozone values from the GAW Izaña station were used to calculate τ_{O_3} (Wehrli, 2008a). If no Brewer data is available, data retrieved from the Total Ozone Mapping Spectrome-
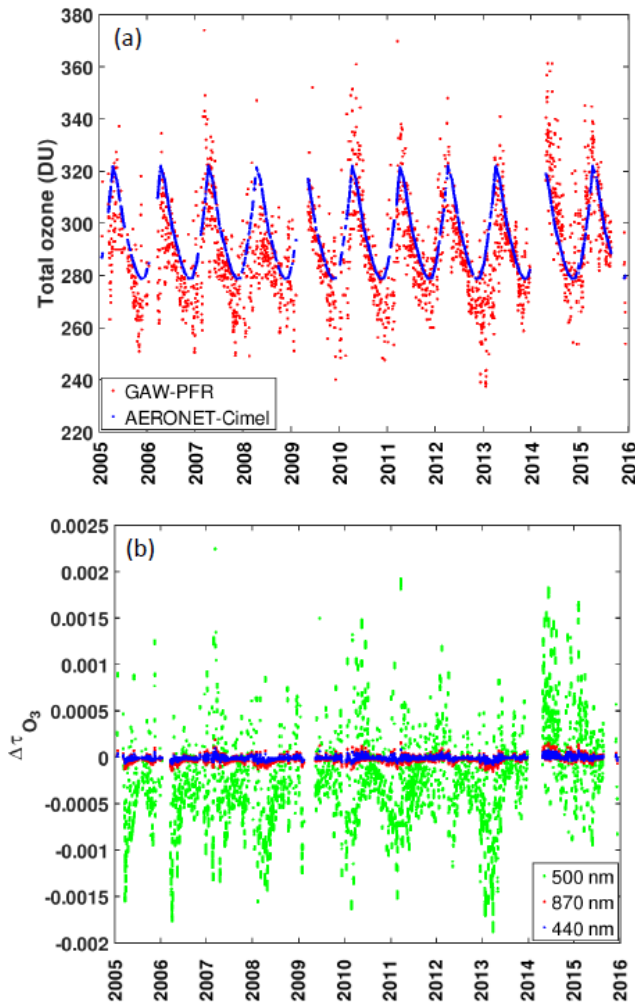
Figure 5. (a) Total O_3 used by GAW-PFR (measured Brewer O_3 values from IZO, OMI O_3 overpass or Brewer O_3 climatology) and AERONET-Cimel (TOMS O_3 climatology) and **(b)** $\Delta\tau_{O_3}(\lambda)$ caused by differences in daily total O_3 between the two instruments in the period 2005–2015.

ter (TOMS) satellite sensor was used. Nowadays, GAW-PFR uses ozone data from AURA satellite overpass observations with the Ozone Monitoring Instrument (OMI) (McPeters et al., 2015) for daily operations (Kazadzis et al., 2018b). Concerning AERONET-Cimel V2, a NASA TOMS $1° × 1.25°$ resolution O_3 climatology is used. From Eq. (10), the differences in O_3 optical depth $\Delta\tau_{O_3}$ can be derived as follows:

$$\Delta\tau_{O_3} = \sigma_{O_3}(\lambda)\frac{1}{1000}\frac{m_{O_3}(O_{3PFR} - O_{3Cimel})}{m_a}. \tag{12}$$

The largest influence of total ozone data uncertainty in τ_{O_3} occurs at 500 nm (Fig. 5). According to Wehrli (2008b) and Kazadzis et al. (2018b), total ozone needs to be determined to ±30 DU or 10 % of typical values to ensure an uncertainty of ~ 0.001 in τ_{O_3} at 500 nm. In the case of the GAW-PFR–

AERONET-Cimel comparison and due to the very different method in which both networks obtained O_3 values for their corresponding corrections, the ozone differences found on some days (1761 out of 71 965 d; 2.4 %) are very large (> 40 DU), exceeding a difference in the ozone optical depth of 0.001. Even so, the potential contribution to AOD differences outside the U_{95} limits between the two networks is negligible. Total O_3 over IZO shows a relatively small amplitude throughout the year but both surface ozone concentrations and column ozone amounts could sharply increase under the influence of cut-off lows injecting air from the high mid-troposphere into the lower subtropical troposphere, which is not uncommon in spring and the first half of summer (Cuevas et al., 2015; Kentarchos et al., 2000). In addition, the upper and middle troposphere could be enriched in ozone through exchange processes in the upper troposphere–lower stratosphere (UTLS) due to the presence of the subtropical jet (mainly from February to April) (Rodriguez-Franco and Cuevas, 2013). However, if we wanted to repeat this traceability study of 1 min AOD data at middle- or high-latitude stations where sharp O_3 variations (several tens of DU) could be registered in a few hours, the correction of 1 min AOD measurements by τ_{O_3} might be a challenging issue.

Differences in NO_2 absorption

AERONET-Cimel applies a correction by absorption of NO_2, but GAW-PFR does not include this correction. AERONET-Cimel V2 obtains daily total NO_2 data from a $0.25° × 0.25°$ resolution NO_2 monthly climatology obtained from the ESA Scanning Imaging Absorption SpectroMeter for Atmospheric CHartographY (SCIAMACHY) (Eskes and Boersma, 2003). AERONET-Cimel V3 uses a geographic and temporally dependent multiyear monthly climatology from the Ozone Monitoring Instrument (OMI) NO_2 concentration (Giles et al., 2019). In order to assess the contribution to AERONET-Cimel 1 min AOD data non-traceability by NO_2 absorption, we have to estimate the NO_2 optical depth ($\tau_{NO_2}(\lambda)$) of AERONET-Cimel since GAW-PFR does not perform this correction. Analogous to $\Delta\tau_{O_3}$, the differences in nitrogen dioxide optical depth $\Delta\tau_{NO_2}$ can be obtained from the following equation:

$$\Delta\tau_{NO_2} = \sigma_{NO_2}(\lambda)\frac{1}{1000}\frac{m_{NO_2}}{m_a}(-NO_{2Cimel}), \tag{13}$$

where m_a is given by Eq. (7), NO_{2Cimel} (DU) is the daily total NO_2 used by AERONET-Cimel and $\sigma_{NO_2}(\lambda)$ is the NO_2 absorption (Gueymard, 1995) weighted by the specific filter response: 15.6 cm^{-1} (380 nm), 12.3 cm^{-1} (440 nm) and 4.62 cm^{-1} (500 nm). Finally m_{NO_2} has the following expression (Gueymard, 1995):

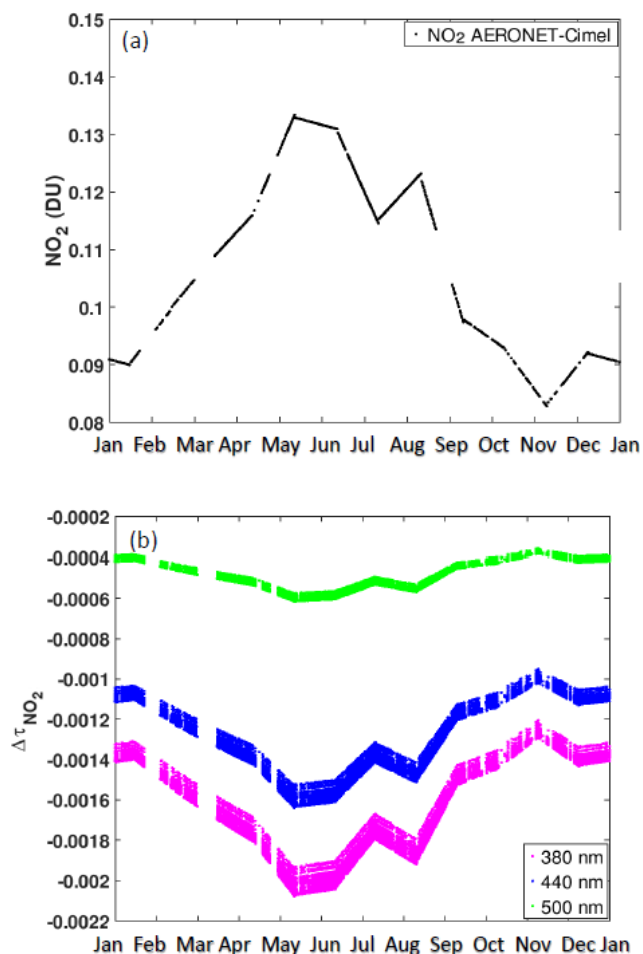$$m_{NO_2} = \frac{1}{\sin\theta + 602.30(90 - \theta)^{0.5}(27.96 + \theta)^{-3.4536}}. \tag{14}$$

Figure 6. **(a)** NO_2 monthly climatology obtained from the ESA SCanning Imaging Absorption SpectroMeter for Atmospheric CHartographY (SCIAMACHY), used by AERONET-Cimel at IZO, and **(b)** $\Delta\tau_{NO_2}$ caused by differences in daily total NO_2 between GAW-PFR and AERONET-Cimel in the period 2005–2015. Note that GAW-PFR does not take into account the correction for the NO_2 absorption.

In Fig. 6a the total NO_2 used by AERONET-Cimel to evaluate $\sigma_{NO_2}(\lambda)$ is depicted. Figure 6b shows the $\Delta\tau_{NO_2}$ caused by differences in daily total NO_2 between GAW-PFR and AERONET-Cimel. $\Delta\tau_{NO_2}$ is of the order of 10^{-3} for the 380 and 440 nm channels, while for the 500 nm channel it is of the order of 10^{-4}. However, it should be noted that an impact on AOD calculation is expected when replicating similar analysis in highly NO_2 polluted regions. Such cases include large industrial cities from East Asia and Central and Eastern Europe (e.g. Chubarova et al., 2016).

Taking into account the corrections for Rayleigh scattering and for the absorptions by O_3 and NO_2, we have calculated the additional traceable AOD data (Table 9). This percentage is at a maximum at 380 nm with 1.3 % (V2) and 1.7 % (V3) of the whole dataset. The 870 nm channel is only affected by the

Table 9. Percentage (%) of additional traceable AERONET-Cimel AOD 1 min data (V2 and V3) after correcting for pressure and total column O_3 and NO_2 for the period 2005–2015.

Channel	Increment (%) of traceable AOD data after P, O_3 and NO_2 corrections	
	V2	V3
380 nm	1.3	1.7
440 nm	0.2	0.3
500 nm	0.3	0.1
870 nm	~ 0.0	~ 0.1

Table 10. Percentage of AERONET V2 AOD data outside the U_{95} limits at 380, 440, 500 and 870 nm channels and for three $AOD_{500\,nm}$ thresholds with respect to all data and with respect to all data for each AOD interval (in brackets).

	Percentage of AOD data outside the U_{95} limits (%)		
	$AOD_{500\,nm} > 0.1$	$AOD_{500\,nm} > 0.2$	$AOD_{500\,nm} > 0.3$
380 nm	1.9 (25.0)	1.2 (47.2)	0.5 (59.8)
440 nm	1.0 (13.5)	0.8 (32.0)	0.5 (57.6)
500 nm	0.6 (8.0)	0.5 (18.7)	0.3 (39.3)
870 nm	0.3 (4.1)	0.2 (6.4)	0.1 (14.0)

Rayleigh correction component, and therefore the increment of traceable data after the mentioned corrections is minimal.

5.4 GAW PFR and AERONET-Cimel comparison under high AOD conditions: the impact of dust forward scattering for different FOVs

When we present the AOD differences between AERONET-Cimel and GAW-PFR versus AOD (GAW-PFR) for AOD > 0.1 (dusty conditions), we note that AERONET-Cimel shows slightly higher AOD values than GAW-PFR (Fig. 7). Similar results for V3 are shown in S12. In fact, the percentage of data outside the U_{95} limits increases as AOD increases (Table 10), thus for dust-related aerosol conditions ($AOD_{500\,nm} > 0.3$) the percentage of AOD data outside the U_{95} limits is > 50 % for 380 and 440 nm (Table 10, percentages in brackets). Similar results are found when using AERONET V3 (see Supplement S13). Taking into account the number of data compared with the total cases, these results show a small but non-negligible percentage of AOD differences outside the U_{95} limits for AOD > 0.1, ranging from ~ 0.3 % at 870 to ~ 1.9 % at 380 nm (Table 10).

Aerosol forward scattering within the FOV of various instruments and calculated AOD was investigated some decades ago by Grassl (1971), who determined that at AOD = 1 and the circumsolar radiation increases the incoming radiation by > 10 %. Russell et al. (2004), using dust and marine aerosols data, quantified the effect of diffuse light for common sun photometer FOV. They reported that the correc-
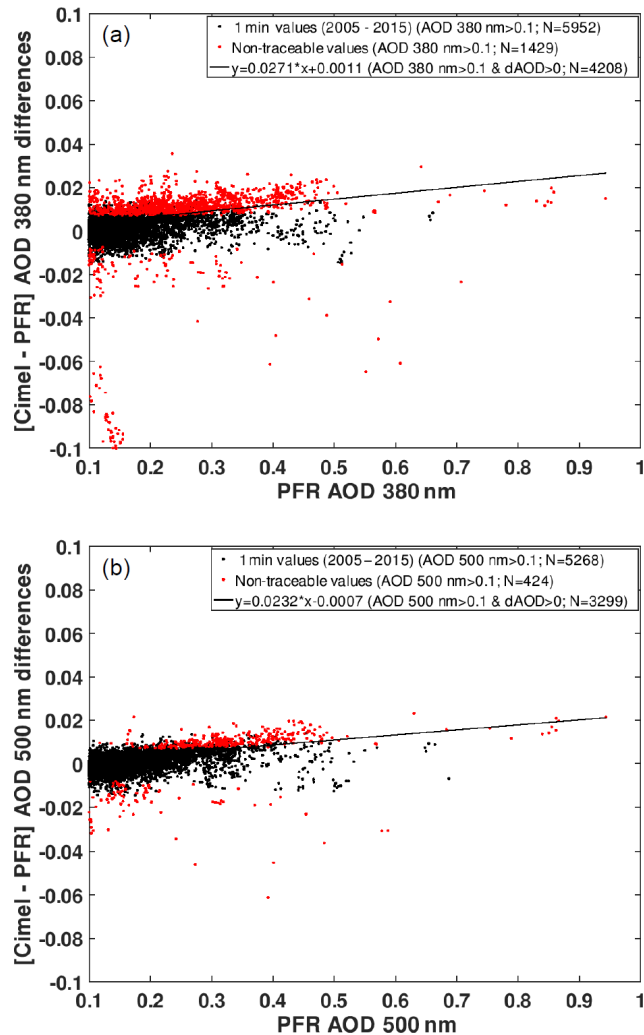
Figure 7. Actual AOD differences between AERONET-Cimel V2 and GAW-PFR versus AOD_{PFR} at **(a)** 380 nm **(b)** and 500 nm for the period 2005–2015. The fitting line has been calculated with those data points with AOD > 0.1 and Cimel–PFR AOD difference > 0. The number of data used in the plots is indicated in the legend. The percentage of non-traceable AOD data with these conditions is ∼ 24 % for 380 nm and ∼ 8 % for 500 nm. Note that some traceable (black) points show larger AOD differences than non-traceable (red) points because of the air mass dependence of the WMO traceability criterion.

tion to AOD is negligible (< 1 % of AOD) for sun photometers with narrow FOV (< 2°), which is greater than the Cimel FOV and slightly smaller than the PFR FOV (2.5°). Sinyuk et al. (2012) assessed the impact of the forward-scattering aerosol on the uncertainty of the AERONET AOD, concluding that only dust aerosol with high AOD and low solar elevation could cause a significant bias in AOD (> 0.01).

GAW-PFR has double the FOV (2.5°; Wehrli, 2000) compared to the AERONET-Cimel (1.3° ± 4.8 %; Torres et al., 2013), so it is reasonable to expect that it is more affected

by the circumsolar radiation than the AERONET-Cimel radiometer. Taking advantage of the fact that Saharan dust intrusions regularly affect IZO, we provide a detailed analysis on the impact that dust forward scattering causes on the AOD retrieval of the two radiometers with different FOV, explaining the AOD differences under moderate-to-high dust load (AOD > 0.1) conditions. For this purpose we have used a forward Monte Carlo model (see Sect. 4.4) with which we perform simulations that include accurate dust aerosol near-forward-scattering effects.

Dust aerosol single-scattering properties were computed using Mie theory, assuming a refractive index of $1.47 + 0.0025i$ at the wavelengths of 380, 440 and 500 nm and $1.46 + 0.012i$ at 870 nm, based on AERONET measurements at IZO. Seven values of aerosol effective radius (r_e) in the range 0.2 to 3.0 µm were considered and a lognormal size distribution with a geometric standard deviation of 2 was assumed. A middle-latitude summer atmospheric profile starting from the Izaña altitude (2.4 km a.s.l.) was assumed, with the aerosol layer located at 5–6 km a.s.l. (typical of summertime). A spectrally uniform surface albedo of 0.11 was employed. Computations were performed for nine AOD values (AOD = 0, 0.1, 0.2, 0.3, 0.4, 0.5, 0.6, 0.8 and 1.0) and for five solar elevation angles ($\theta = 80, 60, 45, 30$ and $20°$). The Monte Carlo model assumes a plane-parallel atmosphere, so the air mass factor is $m = 1/\sin\theta$. A total of 10 million photons were used for each case and wavelength.

Supplement S14 shows the ratio of scattered to direct radiation for cases with AOD up to 0.5. The ratio increases with increasing r_e, as the aerosol forward-scattering peak grows stronger. In the case of Saharan dust intrusions at IZO, the median r_e determined from both AERONET data inversion and the in situ aerodynamic particle sizer (APS) analyser is ∼ 1.5 µm. This value agrees with the dust size distribution found during SAMUM-2 during long-range transport regime (Weinzierl et al., 2011). For this particle size, the ratio of scattered to direct radiation is ∼ 3 times larger for FOV of 2.5° than FOV of 1.3°.

The error in the retrieved AOD due to scattered radiation within the instrument FOV was evaluated by comparing the apparent AODs, defined as follows:

$$AOD_{app,PFR} = -\frac{1}{m}\ln\frac{F_{PFR}}{F_{PFR}(AOD=0)}, \qquad (15)$$

$$AOD_{app,Cimel} = -\frac{1}{m}\ln\frac{F_{Cimel}}{F_{Cimel}(AOD=0)}, \qquad (16)$$

with the true AOD

$$AOD_{true} = -\frac{1}{m}\ln\frac{F_{dir}}{F_{dir}(AOD=0)}, \qquad (17)$$

where F_{dir} is the irradiance due to direct (i.e. non-scattered) radiation and F_{PFR} (F_{Cimel}) is the total irradiance that would be measured by the PFR (Cimel) radiometer, considering the

instrument FOV and the FOV angular function. The relative error in AOD depends strongly on the particle size but it is fairly constant for each r_e value considered (see Supplement S15). For $r_e \sim 1.5\,\mu m$, the relative error in AOD at 380 nm (500 nm) is $\sim 1.6\,\%$ (1.0 %) for Cimel and $\sim 5\,\%$ ($\sim 3\,\%$) for PFR. These errors are in good agreement with those estimated by Russell et al. (2004) and slightly higher than the relative AOD error of 0.7 % due to coarse dust aerosol forward scattering reported by Eck et al. (1999).

The Monte Carlo simulated relative differences in retrieved AOD (in percentage) that would result from the scattered radiation within the FOV of the PFR and Cimel instruments and the difference in retrieved AOD between PFR and Cimel as a function of the AOD retrieved with PFR, for 380 and 500 nm, are shown in Fig. 8. The main results of these simulations are that (1) the higher FOV of the PFR, compared to that of the Cimel, results in lower AOD values for the PFR and (2) the fractional AOD difference related to the different FOVs of PFR and Cimel is fairly constant for any aerosol effective radius but increases with increasing the effective radius. This fact might explain at least some of the systematic differences seen in Fig. 7. Note that, as lower AOD values derived from the PFR are expected based on its larger FOV, the linear fits in Fig. 7 have been calculated for those data points with the Cimel–PFR AOD differences > 0. In this way, we discard those pairs of AOD data, whose difference is not only due to the different FOV between both instruments, thus obtaining a better approximation to quantify this effect.

The slopes of the fitting lines of the Cimel–PFR AOD differences versus PFR AOD for AOD > 0.1 (dusty conditions) are 2.7 % for 380 nm and 2.3 % for 500 nm (Fig. 7), which are quite consistent with the percentage differences of AOD between Cimel and PFR for an effective radius of 1.5 μm (Fig. 8a and b). These percentages correspond to absolute AOD differences of 0.016 at 380 nm and 0.011 at 500 nm for AOD = 0.5 (Fig. 8c and d), which are of sufficient magnitude to cause an appreciable number of 1 min AOD data outside the U_{95} limits, as indicated in Table 10.

If we apply the corresponding corrections to the 1 min AOD PFR data > 0.1 assuming an effective radius of 1.5 μm, +3.3 % at 380 nm and +2.2 % at 500 nm, it turns out that the slopes of the fitting lines of the Cimel–PFR AOD differences versus PFR AOD become practically zero (Fig. 9). Moreover, the number of AOD data outside the U_{95} limits is reduced by approximately 53 % for 380 nm and by 13 % for 500 nm. It must be taken into account that the percentage of AOD data for AOD > 0.1 outside the U_{95} limits, before the corrections, is only 8 % at 500 nm, while at 380 nm it is a significant value (24 %).

This AOD "correction" reduces the Cimel–PFR AOD differences substantially but does not eliminate them completely. The main reason is the inherent limitation of data correction using the percentage difference in AOD obtained by model simulation for a fixed effective radius. We have assumed an effective radius of 1.5 μm but, in reality, the radius

of dust particles varies. A reasonable range of dust particle radii is between 0.1 and 3 μm (Balkanski et al., 1996; Denjean et al., 2016; Mahowald et al., 2014). So, depending on the distance from the dust source to IZO and the size of the emitted dust, the effective radius could vary slightly between dust episodes. As can be seen in Fig. 8a and b, the percentage differences in AOD between Cimel and PFR for a 1–2 μm effective radius interval, i.e. the Cimel–PFR AOD relative difference at 380 nm (500 nm), might change between $\sim -1.8\,\%$ (−1.1 %) to −4.9 % (3.3 %).

A similar analysis has been carried out for AERONET V3 (see Supplement S16), where we observe that the corrections obtained are not as good as those obtained for V2. The effect of FOV on AOD retrieval should be taken into account for those radiometers with a relatively high FOV ($> 3°$) measuring in regions with relatively high AOD (> 0.2) for most of the year, as is the case in many sites in northern Africa, the Middle East and East Asia (Basart et al., 2009; Cuevas et al., 2015; Eck et al., 1999; Kim et al., 2007). This effect leads to AOD underestimation, and the variable number of high AOD episodes in each season of the year might affect the AOD long-term trends. AOD measurements under these conditions would be especially affected for optical air mass < 3.

5.5 Ångström exponent comparison

We have performed a comparison of the AE provided by GAW-PFR and AERONET-Cimel, using the AOD data obtained from the four common channels (380, 440, 500 and 870 nm) with a total of 70 716 data pairs in both cases. The PFR-AOD values have been ordered from lowest to highest by grouping them in intervals of 500 values for which the averages (and corresponding standard deviations) of the Cimel–PFR AE differences have been calculated (Fig. 10a). We proceeded with the PFR-AE values in a similar way (Fig. 10b).

AE differences > 0.2 increase exponentially for AOD < 0.02, reaching AE differences of up to 1.6 under pristine conditions (Fig. 10a). For very low AOD the provided instrument's uncertainty is the source of the sharp increase in AE and, at the same time, AE becomes very sensitive to slight AOD changes. However, for AOD < 0.02 the atmospheric aerosol load is practically zero and so its characterization with AE has relatively minor importance in practice .

In addition, the AE differences remain < 0.1 when AE_{PFR} values are < 1 (Fig. 10b), which shows that these differences are small in most of the possible atmospheric scenarios. For $1 < AE_{PFR} < 1.2$ the AE differences increase slightly to values < 0.2 and for $AE_{PFR} > 1.2$ (very fine particles or pristine conditions) the AE differences increase sharply to reach values of ~ 1.2. In our case, the non-pristine conditions, or those with a high content of mineral dust, have associated AOD > 0.03 and AE < 1, where the AE differences remain < 0.1. In the case of pristine conditions, AOD ≤ 0.03 and
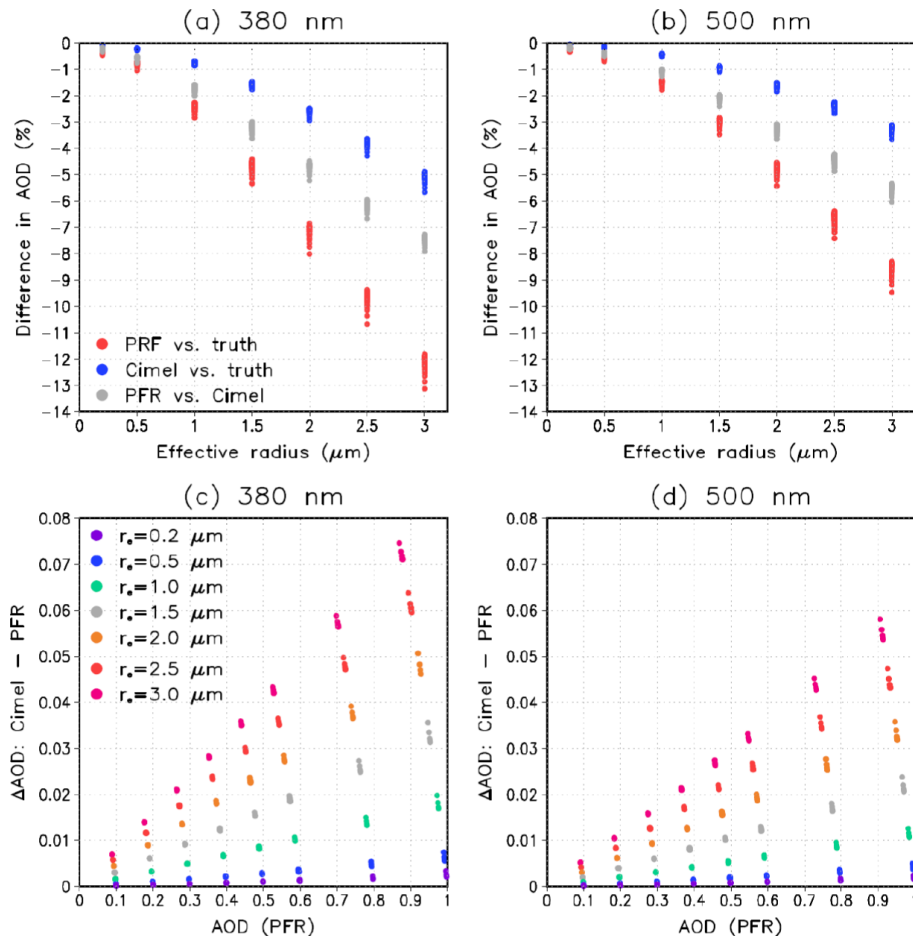
Figure 8. (a, b) The simulated relative differences in retrieved AOD (in percentage) that would result from the scattered radiation within the FOV of the PFR and Cimel instruments. The red (blue) dots show the differences between the AOD that would be retrieved using PFR (Cimel) and the actual AOD and the grey dots show the difference between PFR and Cimel at the **(a)** 380 nm and **(b)** 500 nm wavelengths.**(c, d)** The difference in retrieved AOD between PFR and Cimel, plotted as a function of the AOD retrieved with PFR, for seven values of aerosol effective radius between 0.2 and 3.0 μm at **(c)** 380 and **(d)** 500 nm.

$AE \geq 1$, the AE differences can reach a maximum of 1.6. Wagner and Silva (2008) estimated the usual maximum AE error via error propagation using a pair of spectral channels in which AOD is measured. Their results show that for clean optical conditions ($AOD_{440\,nm} = 0.06$) the maximum AE error is 1.17 and for hazy conditions ($AOD_{440\,nm} = 0.17$) the error is 0.17, assuming an underlying AE of 1.5. These values decrease to 0.73 and 0.11, respectively, if $AE = 0$. The AE differences found between GAW-PFR and AERONET-Cimel lie within the estimated errors reported by Wagner and Silva (2008).

In any case, as in our study, the AE has been determined from AOD measured in the four common channels of GAW-PFR and AERONET-Cimel, we estimated the uncertainty in the calculation of the AE for three typical aerosol scenarios at Izaña. Following the methodology shown by Wagner and Silva (2008), the AE uncertainty estimations have been calculated using AOD measurements at four wavelengths and

Table 11. Uncertainty in AE determination for three typical atmospheric situations.

	Uncertainty in AE
Normal pristine conditions $AOD_{500\,nm} = 0.03$ and $AE = 1.4$	≥ 1
Hazy conditions $AOD_{500\,nm} = 0.14$ and $AE = 1.15$	≥ 0.2
Strong dust intrusion $AOD_{500\,nm} = 0.3$ and $AE = 0.3$	~ 0

AOD uncertainty error propagation (Table 11). The AE derived from more than two wavelengths is less affected by AOD uncertainties than AE calculated with pairs of wavelengths, since the latter are calculated from the ratio of AOD at two channels (Cachorro et al., 2008).
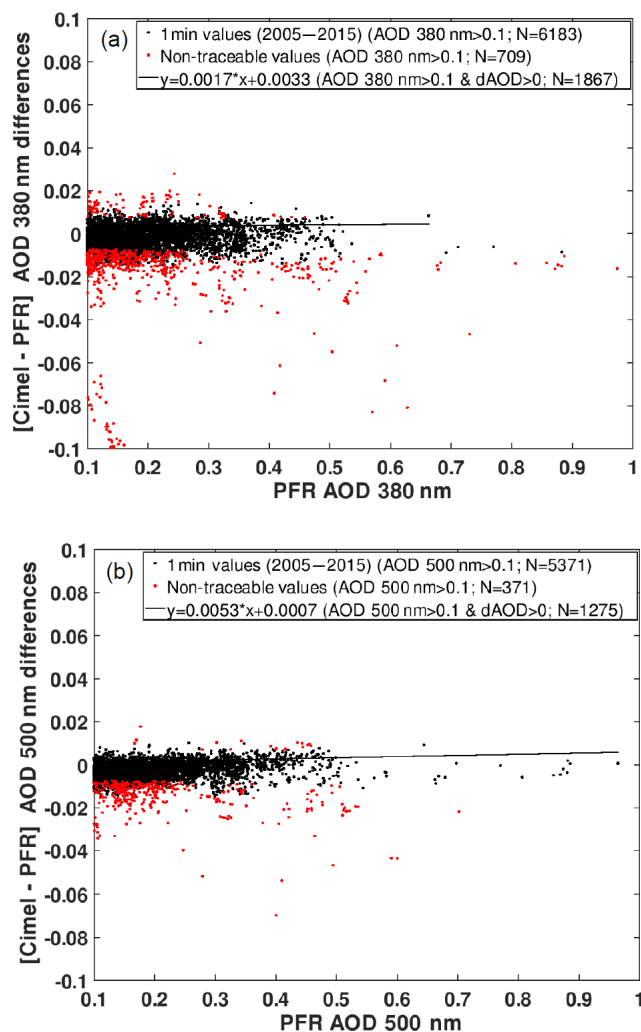
Figure 9. The same as Fig. 7 after correcting the PFR AOD data by adding $+3.3\%$ at 380 nm and $+2.2\%$ at 500 nm to the 1 min PFR AOD data > 0.1.
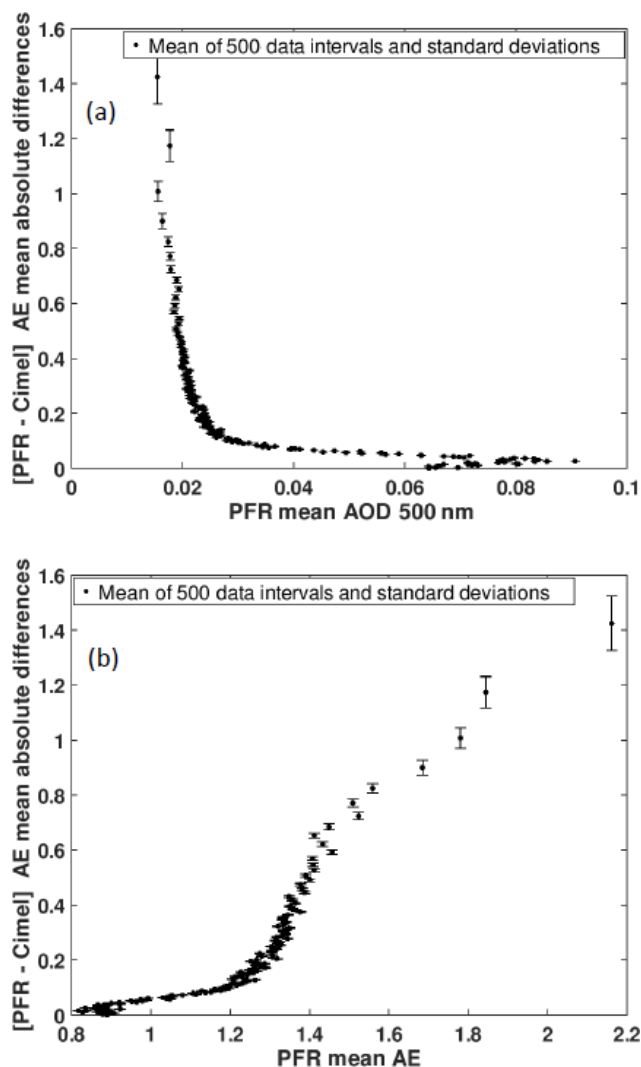

Figure 10. (a) Cimel–PFR AE mean absolute differences (and corresponding standard deviations) versus PFR mean $AOD_{500\,nm}$ in 500 data intervals **(b)** and versus PFR mean AE in 500 data intervals. AE has been computed for both PFR and Cimel using the four common channels (380, 440, 500 and 870 nm).

The AE differences of our study (Fig. 10) are within the AE uncertainty estimated for each type of atmospheric condition (pristine, hazy and heavily dust loaded). However, although AE is a quantitative parameter, it is only used in a qualitative way to estimate the range of sizes (fine, medium, coarse) of the predominant aerosol in the inevitable mixture of aerosols that we observe. With this parameter, together with the information that is available in the measurement site about the most frequent types of aerosols and their concentration, we can estimate the type of aerosols that are being measured. There are many publications with different thresholds of AE and AOD in order to classify different types of aerosols (e.g. Basart et al., 2009; Cuevas et al., 2015; Dubovik et al., 2002; Guirado et al., 2014; Holben et al., 2001; Kim et al., 2007; Todd et al., 2007; Toledano et al., 2007; Wang et al., 2004). However, there is no consensus on these thresholds since at each site there are different mixtures of aerosols

and each type of aerosol shows specific frequencies of appearance and different concentrations. An alternative way of analysing the degree of agreement in AE between GAW-PFR and AERONET-Cimel is to verify to what extent both networks provide the same information regarding the type of aerosol they observe in a certain site.

Considering the AE criteria established by Cuevas et al. (2015) and Berjón et al. (2019), we have identified the following four main categories according to the AE_{PFR} and AE_{Cimel} values:

1. AE_{PFR} and $AE_{Cimel} > 0.6$: pristine conditions.

2. $0.25 < AAE_{PFR}$ and $AE_{Cimel} \leq 0.6$: hazy, mineral dust being the main aerosol component.

3. AE_{PFR} and $AE_{Cimel} \leq 0.25$: pure dust.

4. AE_{PFR} and AE_{Cimel}: does not fit any of the previous categories.

In 94.9 % of the cases, GAW-PFR and AERONET-Cimel V2 match the AE intervals of each aerosol scenario. Similar results (93.4 %) were obtained when comparing with AERONET V3. Most of the agreement (> 80 %) occurs in the predominant scenario of pristine conditions despite the AE uncertainty under pristine conditions being ≥ 1. See Supplement S17 for more details. Note that the choice of these categories is not relevant since this is only used to examine the long-term agreement in AE between GAW-PFR and AERONET-Cimel in different atmospheric conditions.

6   Summary and conclusions

While GAW-PFR is the WMO-defined global AOD reference, being directly linked to WMO-CIMO, and was specifically designed to detect long-term AOD trends, AERONET-Cimel is the densest AOD measurement network globally, and the network most frequently used for aerosol characterization and for model and satellite observation evaluation.

An AERONET-Cimel 11-year AOD data series at IZO was obtained using a large number of radiometers. A total of 13 reference instruments were used in the period 2005–2009, which means that approximately every 4.5 months an instrument was replaced by another one to be calibrated. Their calibrations were performed during their respective measurement time periods at IZO. Therefore, these calibrations were not in any way linked with those of the instruments that preceded or replaced them or with GAW-PFR reference. These facts led us to investigate the homogeneity of the AERONET-Cimel AOD data series and their intercomparability with the much more homogeneous AOD data series from GAW-PFR (three instruments in 11 years). The traceability concept for AOD suggested by WMO consists in determining whether the AOD difference of the AERONET CIMELs versus the GAW PFRs lies within the U_{95} limits. We have used uncertainty limits for AOD traceability established by WMO (2005) for these type of instruments with finite FOV. The acceptable traceability is when 95 % of the absolute AOD differences lie within these limits, in which case both data populations are considered equivalent. It should be clarified that "traceability" is not used in a strict meteorological sense. This study has addressed the comparison of the GAW-PFR dataset with the two versions of AERONET (V2 and V3) in the period 2005–2015. An excellent agreement between V2 and V3 for the four analysed channels ($R^2 > 0.999$) has been obtained.

More than 70 000 synchronous GAW-PFR and AERONET-Cimel 1 min data pairs in each channel in the period 2005–2015 were analysed. An excellent traceability of AOD from the AERONET-Cimel (V2 and V3) is found for 440, 500 and 870 nm as well as fairly good results for 380 nm. The lowest percentage of traceable AOD data is registered at 380 nm, with 92.7 % of the 1 min data within the WMO limits, and the highest at 870 nm, with 98.0 % of the data within the same limits.

The different possible causes of non-traceability in AOD were investigated as follows:

– *Absolute AOD measurements synchronization.*

Analysing 1 min AOD variability, we concluded that its impact on the AOD differences is quite small, as only ~ 0.8 % of the AOD data have a variability larger than 0.005 in all spectral ranges.

– *Sun tracking misalignments.*

Sun tracking misalignments constitute a serious problem and a major cause of non-traceability of AOD data pairs, as demonstrated by the AOD data outside the U_{95} limits from the period 2005–2009, as a consequence of episodic problems with the sun tracker of the GAW-PFR radiometer. For the 2010–2015 period the percentage of traceable data pairs improves to 93.5 % (380 nm), 97.4 % (440 nm), 97.2 % (500 nm) and 99.1 % (870 nm). However, most of these cases could be identified and excluded from the analysis.

– *Cloud screening failure by both network algorithms.*

According to our observations, the simultaneous failure of both cloud screening algorithms might occur only under the presence of large and stable cirrus. In these cases, the radiometers interpret these clouds as aerosol layers and might provide values very different from the real AOD. For the comparison at IZO, however, this effect is negligible since GAW-PFR and AERONET-Cimel cloud screening algorithms provide successful cloud identification of clear direct sun conditions during cloudy skies (FCS < 40 %) for 99.75 % of the cases.

– *Pressure-measurement-related errors.*

Since the accuracy of the new barometers built into new radiometers is about 3 hPa and only errors in atmospheric pressure > 30 hPa might produce an impact on Rayleigh scattering, the AOD non-traceability due to errors in Rayleigh scattering is negligible.

– *Total column ozone input uncertainty.*

The largest influence of total ozone data uncertainty on ozone absorption occurs mainly at 500 nm. Total ozone needs to be determined to ± 30 DU or 10 % of typical values to ensure an uncertainty of ± 0.001 ozone absorption at 500 nm. In the case of the GAW-PFR–AERONET-Cimel comparison, despite the very different methods in which both networks obtained values for their corresponding corrections, large ozone differences were found (> 40 DU) only on 2.4 % of the

days, resulting in a difference in the ozone optical depth slightly above ~ 0.001. The potential contribution to non-traceable AOD values between the two networks is negligible. However, at middle- or high-latitude stations where fast O_3 variations of several tens of DU might be registered, the correction of 1 min AOD measurements by ozone absorption might be an issue to be considered.

– *Total column* NO_2 *input uncertainty.*

The differences in NO_2 absorption caused by differences in daily total NO_2 between GAW-PFR and AERONET-Cimel is of the order of 10^{-3} for 380 and 440 nm channels, while for 500 nm channel it is even lower, of the order of 10^{-4}. Therefore, differences in NO_2 absorption are negligible in the 1 min AOD non-traceability of our study. However, NO_2 absorption might have some impact on AOD in highly polluted regions, such as in large industrial cities, where column NO_2 values are much larger than the climatological ones.

Taking into account the corrections for Rayleigh scattering and for the absorptions by O_3 and NO_2, we have calculated the combined effect of all of them on the non-traceability of the 1 min AOD values. The highest impact occurs in the 380 nm channel, in which 25 % of the AOD data outside the U_{95} limits (~ 2 % of the total compared data) are due to significant differences in pressure and in O_3 and NO_2 absorption. The 1 min AOD data outside the U_{95} limits by these corrections is negligible in the 870 nm channel.

– *Impact of dust forward scattering in AOD retrieval uncertainty for different instrument FOVs.*

Since GAW-PFR has almost double the FOV ($\sim 2.5°$) compared to the AERONET-Cimel ($\sim 1.3°$) and direct solar irradiance measurements are biased by the amount of aureole radiation that is assumed to be direct solar radiation, it is reasonable to expect that the GAW-PFR is more affected by the circumsolar irradiance than the AERONET-Cimel radiometer when AOD is relatively high. Modelling the dust forward scattering we have shown that a non-negligible percentage of the non-traceable 1 min AOD data for AOD > 0.1, ranging from ~ 0.3 % at 870 nm to ~ 1.9 % at 380 nm is caused by the different FOV. Due to this effect, the GAW-PFR provides AOD values, which are ~ 3 % lower at 380 nm and ~ 2 % lower at 500 nm compared with AERONET-Cimel. However, AOD underestimation could only have some relevance in dusty regions if radiometers with relatively large FOV are used.

A comparison of the AE provided by GAW-PFR and AERONET-Cimel has been performed using AOD data obtained from the four nearby common channels with a total of 70 716 data pairs in both cases. This is a very strict AE calculation since it is necessary that AOD be accurately measured by the four channels simultaneously. AE differences > 0.2 increase exponentially under very pristine conditions (AOD ≤ 0.03 and AE ≥ 1), reaching AE differences of up to 1.6. However, for these conditions the atmospheric aerosol load is practically zero and so its characterization with AE does not have any importance in practice. Under non-pristine conditions or those with a high mineral dust content (associated AOD > 0.03 and AE < 1), the AE differences remain < 0.1.

Summarizing, we have presented for the first time a long-term (2005–2015) 1 min AOD comparison among different types of radiometers belonging to different aerosol global networks. This comparison is a very demanding test of both GAW-PFR and AERONET-Cimel validated AOD datasets since aerosol scenarios correspond to extreme conditions: either very low aerosol loading, a "pristine" scenario that reveals small uncertainties in the calibration and in the cloud screening, or large dust load, which leads to a significant increase in the forward-scattering aerosol with AOD, resulting in a slightly higher AOD underestimation by the GAW-PFR. From this comprehensive comparison, we can conclude that both AOD datasets are representative of the same AOD population, which is a remarkable fact for the global aerosol community. It should be noted that AOD traceability at 380 nm (92.7 %) does not reach 95 % of the common data, the percentage recommended by WMO U_{95} criterion, so more efforts should be made to improve AOD in the UV range. In this study we have also investigated the data that are outside of the WMO U_{95} limits in order to understand their causes and to be eventually able to correct the small inconsistencies detected in instrumental and methodological aspects in the future.

Our results suggest that WMO-CIMO traceability limits could be redefined as a function of wavelength and the recommended radiometer FOV range should be reconsidered. The widely deployed AERONET-Cimel and GAW-PFR datasets play a crucial role in understanding long-term AOD changes and detecting trends, so it would be desirable for both networks to be linked to the same WMO-GAW-related reference.

Author contributions. EC, PMR-C, NK and SK conceived and designed the structure and methodology of the paper and wrote the main part of the manuscript, coordinated by EC. PMR-C evaluated the AERONET V2 and V3 1 min AOD and AE data and performed the data comparison with GAW-PFR. NK processed the quality assured GAW-PFR 1 min AOD and AE data, analysed the short-term AOD natural variability from the GAW-PFR 1 min AOD data and was in charge of the GAW-PFR radiometer calibrations. PR performed and discussed the modelling results with the Monte Carlo forward model. RDG contributed to the dust forward-scattering section and prepared the paper edition in Latex. AB obtained the results of the 1 min AOD natural variability from the Cimel Triplets. CG-F was responsible for the careful calibration of Cimel Masters. RDG, AB, CG-F and PMR-C participated actively in the analysis of the case studies shown in the Supplement. RR has coordinated the maintenance and daily checks of the PFR and Cimel radiometers since 2005, resolving technical and logistical problems. CT contributed to the GAW-PFR and AERONET-Cimel calibration aspects addressed in the paper. FA provided detailed information of the Cimel radiometers, taking care of their complex technical problems. JG contributed with concepts of traceability and comparability used in the paper. All authors discussed the results and contributed to the final paper. EC and SK supervised this research activity.

Competing interests. The authors declare that they have no conflict of interest.

References

Amiridis, V., Marinou, E., Tsekeri, A., Wandinger, U., Schwarz, A., Giannakaki, E., Mamouri, R., Kokkalis, P., Binietoglou, I., Solomos, S., Herekakis, T., Kazadzis, S., Gerasopoulos, E., Proestakis, E., Kottas, M., Balis, D., Papayannis, A., Kontoes, C., Kourtidis, K., Papagiannopoulos, N., Mona, L., Pappalardo, G., Le Rille, O., and Ansmann, A.: LIVAS: a 3-D multi-wavelength aerosol/cloud database based on CALIPSO and EARLINET, Atmos. Chem. Phys., 15, 7127–7153, https://doi.org/10.5194/acp-15-7127-2015, 2015.

Ångström, A.: On the atmospheric transmission of sun radiation and on dust in the air, Geogr. Ann., 11, 156–166, 1929.

Balkanski, Y., Schulz, M., Marticorena, B., Bergametti, G., Guelle, W., Dulac, F., Moulin, C., and Lambert, C.: Importance of the source term and of the size distribution to model the mineral dust cycle, in: The impact of desert dust across the Mediterranean, 69–76, Springer, https://doi.org/10.1007/978-94-017-3354-0_6, 1996.

Barker, H. W.: Solar radiative transfer through clouds possessing isotropic variable extinction coefficient, Q. J. Roy. Meteor. Soc., 118, 1145–1162, https://doi.org/10.1002/qj.49711850807, 1992.

Barker, H. W.: Estimating cloud field albedo using one-dimensional series of optical depth, J. Atmos. Sci., 53, 2826–2837, https://doi.org/10.1175/1520-0469(1996)053<2826:ECFAUO>2.0.CO;2, 1996.

Barreto, A., Cuevas, E., Pallé, P., Romero, P. M., Guirado, C., Wehrli, C. J., and Almansa, F.: Recovering long-term aerosol optical depth series (1976–2012) from an astronomical potassium-based resonance scattering spectrometer, Atmos. Meas. Tech., 7, 4103–4116, https://doi.org/10.5194/amt-7-4103-2014, 2014.

Barreto, Á., Cuevas, E., Granados-Muñoz, M.-J., Alados-Arboledas, L., Romero, P. M., Gröbner, J., Kouremeti, N., Almansa, A. F., Stone, T., Toledano, C., Román, R., Sorokin, M., Holben, B., Canini, M., and Yela, M.: The new sun-sky-lunar Cimel CE318-T multiband photometer – a comprehensive performance evaluation, Atmos. Meas. Tech., 9, 631–654, https://doi.org/10.5194/amt-9-631-2016, 2016.

Basart, S., Pérez, C., Cuevas, E., Baldasano, J. M., and Gobbi, G. P.: Aerosol characterization in Northern Africa, Northeastern Atlantic, Mediterranean Basin and Middle East from direct-sun AERONET observations, Atmos. Chem. Phys., 9, 8265–8282, https://doi.org/10.5194/acp-9-8265-2009, 2009.

Basart, S., Pérez, C., Nickovic, S., Cuevas, E., and Baldasano, J.: Development and evaluation of the BSC-DREAM8b dust regional model over Northern Africa, the

Mediterranean and the Middle East, Tellus B, 64, 18539, https://doi.org/10.3402/tellusb.v64i0.18539, 2012.

Benedetti, A., Reid, J. S., Knippertz, P., Marsham, J. H., Di Giuseppe, F., Rémy, S., Basart, S., Boucher, O., Brooks, I. M., Menut, L., Mona, L., Laj, P., Pappalardo, G., Wiedensohler, A., Baklanov, A., Brooks, M., Colarco, P. R., Cuevas, E., da Silva, A., Escribano, J., Flemming, J., Huneeus, N., Jorba, O., Kazadzis, S., Kinne, S., Popp, T., Quinn, P. K., Sekiyama, T. T., Tanaka, T., and Terradellas, E.: Status and future of numerical atmospheric aerosol prediction with a focus on data requirements, Atmos. Chem. Phys., 18, 10615–10643, https://doi.org/10.5194/acp-18-10615-2018, 2018.

Berjón, A., Barreto, A., Hernández, Y., Yela, M., Toledano, C., and Cuevas, E.: A 10-year characterization of the Saharan Air Layer lidar ratio in the subtropical North Atlantic, Atmos. Chem. Phys., 19, 6331–6349, https://doi.org/10.5194/acp-19-6331-2019, 2019.

Bodhaine, B. A., Wood, N. B., Dutton, E. G., and Slusser, J. R.: On Rayleigh optical depth calculations, J. Atmos. Ocean. Tech., 16, 1854–1861, 1999.

Böhm-Vitense, E.: Introduction to stellar astrophysics, Vol. 2. Stellar atmospheres, Cambridge University Press, Cambridge (UK), 12+ 245 p., ISBN 0-521-34403-4, 1989.

Bokoye, A., Royer, A., O'Neil, N., Cliche, P., Fedosejevs, G., Teillet, P., and McArthur, L.: Characterization of atmospheric aerosols across Canada from a ground-based sunphotometer network: AEROCAN, Atmos. Ocean, 39, 429–456, https://doi.org/10.1080/07055900.2001.9649687, 2001.

Cachorro, V., Toledano, C., Sorribas, M., Berjón, A., De Frutos, A., and Laulainen, N.: An "in situ" calibration-correction procedure (KCICLO) based on AOD diurnal cycle: Comparative results between AERONET and reprocessed (KCICLO method) AOD-alpha data series at El Arenosillo, Spain, J. Geophys. Res.-Atmos., 113, D02207, https://doi.org/10.1029/2007JD009001, 2008.

Cachorro, V. E., Romero, P. M., Toledano, C., Cuevas, E., and de Frutos, A. M.: The fictitious diurnal cycle of aerosol optical depth: A new approach for "in situ" calibration and correction of AOD data series, Geophys. Res. Lett., 31, L12106, https://doi.org/10.1029/2004GL019651, 2004.

Campanelli, M., Nakajima, T., and Olivieri, B.: Determination of the solar calibration constant for a sun-sky radiometer: proposal of an in-situ procedure, Appl. Opt., 43, 651–659, 2004.

Carlund, T., Kouremeti, N., Kazadzis, S., and Gröbner, J.: Aerosol optical depth determination in the UV using a four-channel precision filter radiometer, Atmos. Meas. Tech., 10, 905–923, https://doi.org/10.5194/amt-10-905-2017, 2017.

Carrillo, J., Guerra, J. C., and Cuevas, E., and Barrancos, J.: Characterization of the Marine Boundary Layer and the Trade-Wind Inversion over the Sub-tropical North Atlantic, Bound.-Lay. Meteorol., 158, 311–330, https://doi.org/10.1007/s10546-015-0081-1, 2016.

Che, H., Zhang, X.-Y., Xia, X., Goloub, P., Holben, B., Zhao, H., Wang, Y., Zhang, X.-C., Wang, H., Blarel, L., Damiri, B., Zhang, R., Deng, X., Ma, Y., Wang, T., Geng, F., Qi, B., Zhu, J., Yu, J., Chen, Q., and Shi, G.: Ground-based aerosol climatology of China: aerosol optical depths from the China Aerosol Remote Sensing Network (CARSNET) 2002–2013, Atmos. Chem. Phys., 15, 7619–7652, https://doi.org/10.5194/acp-15-7619-2015, 2015.

Chedin, A., Capelle, V., and Scott, N.: Detection of IASI dust AOD trends over Sahara: How many years of data required?, Atmos. Res., 212, 120–129, https://doi.org/10.1016/j.atmosres.2018.05.004, 2018.

Chubarova, N. Y., Poliukhov, A. A., and Gorlova, I. D.: Long-term variability of aerosol optical thickness in Eastern Europe over 2001–2014 according to the measurements at the Moscow MSU MO AERONET site with additional cloud and NO$_2$ correction, Atmos. Meas. Tech., 9, 313–334, https://doi.org/10.5194/amt-9-313-2016, 2016.

Cuevas, E., González, Y., Rodríguez, S., Guerra, J. C., Gómez-Peláez, A. J., Alonso-Pérez, S., Bustos, J., and Milford, C.: Assessment of atmospheric processes driving ozone variations in the subtropical North Atlantic free troposphere, Atmos. Chem. Phys., 13, 1973–1998, https://doi.org/10.5194/acp-13-1973-2013, 2013.

Cuevas, E., Camino, C., Benedetti, A., Basart, S., Terradellas, E., Baldasano, J. M., Morcrette, J. J., Marticorena, B., Goloub, P., Mortier, A., Berjón, A., Hernández, Y., Gil-Ojeda, M., and Schulz, M.: The MACC-II 2007–2008 reanalysis: atmospheric dust evaluation and characterization over northern Africa and the Middle East, Atmos. Chem. Phys., 15, 3991–4024, https://doi.org/10.5194/acp-15-3991-2015, 2015.

Cuevas, E., Gómez-Peláez, A., Rodríguez, S., Terradellas, E., Basart, S., García, R., García, O., and Alonso-Pérez, S.: The pulsating nature of large-scale Saharan dust transport as a result of interplays between mid-latitude Rossby waves and the North African Dipole Intensity, Atmos. Environ., 167, 586–602, https://doi.org/10.1016/j.atmosenv.2017.08.059, 2017a.

Cuevas, E., Milford, C., Bustos, J. J., del Campo-Hernández, García, O., D., G. R., Gómez-Peláez, Guirado-Fuentes, C., Marrero, C., Prats, N., Ramos, R., Redondas, A., Reyes, E., Rodríguez, S., Romero-Campos, P., Scheneider, M., Belmonte, J., Yela, M., Almansa, F., Barreto, A., López-Solano, C., Basart, S., Terradellas, E., Afonso, S., Bayo, C., Berjón, A., Bethencourt, J., Carreño, V., Castro, N. J., Cruz, A. M., Damas, M., De Ory-Ajamil, F., García, M. I., Gómez-Trueba, V., González, Y., Hernández, C., Hernández, Y., Hernández-Cruz, B., Jover, M., León, S., López-Fernández, R., López-Solano, J., Rodríguez, E., Rodríguez-Franco, J., Rodríguez-Valido, M., Sálamo, C., Sanromá, E., Santana, D., Santo-Tomás, F., Sepúlveda, E., Sierra, M., and Sosa, E.: Izaña Atmospheric Research Center Activity Report 2015–2016, State Meteorological Agency (AEMET), 2017b.

Denjean, C., Cassola, F., Mazzino, A., Triquet, S., Chevaillier, S., Grand, N., Bourrianne, T., Momboisse, G., Sellegri, K., Schwarzenbock, A., Freney, E., Mallet, M., and Formenti, P.: Size distribution and optical properties of mineral dust aerosols transported in the western Mediterranean, Atmos. Chem. Phys., 16, 1081–1104, https://doi.org/10.5194/acp-16-1081-2016, 2016.

Driemel, A., Augustine, J., Behrens, K., Colle, S., Cox, C., Cuevas-Agulló, E., Denn, F. M., Duprat, T., Fukuda, M., Grobe, H., Haeffelin, M., Hodges, G., Hyett, N., Ijima, O., Kallis, A., Knap, W., Kustov, V., Long, C. N., Longenecker, D., Lupi, A., Maturilli, M., Mimouni, M., Ntsangwane, L., Ogihara, H., Olano, X., Olefs, M., Omori, M., Passamani, L., Pereira, E. B., Schmithüsen,

H., Schumacher, S., Sieger, R., Tamlyn, J., Vogt, R., Vuilleu-mier, L., Xia, X., Ohmura, A., and König-Langlo, G.: Base-line Surface Radiation Network (BSRN): structure and data description (1992–2017), Earth Syst. Sci. Data, 10, 1491–1501, https://doi.org/10.5194/essd-10-1491-2018, 2018.

Dubovik, O., Holben, B., Eck, T. F., Smirnov, A., Kaufman, Y. J., King, M. D., Tanré, D., and Slutsker, I.: Variability of absorption and optical properties of key aerosol types observed in worldwide locations, J. Atmos. Sci., 59, 590–608, https://doi.org/10.1175/1520-0469(2002)059<0590:VOAAOP>2.0.CO;2, 2002.

Eck, T., Holben, B., Reid, J., Dubovik, O., Smirnov, A., O'neill, N., Slutsker, I., and Kinne, S.: Wavelength dependence of the optical depth of biomass burning, urban, and desert dust aerosols, J. Geophys. Res.-Atmos., 104, 31333–31349, https://doi.org/10.1029/1999JD900923, 1999.

Eskes, H. J. and Boersma, K. F.: Averaging kernels for DOAS total-column satellite retrievals, Atmos. Chem. Phys., 3, 1285–1291, https://doi.org/10.5194/acp-3-1285-2003, 2003.

Freidenreich, S. and Ramaswamy, V.: A new multiple-band solar radiative parameterization for general circulation models, J. Geophys. Res.-Atmos., 104, 31389–31409, https://doi.org/10.1029/1999JD900456, 1999.

García, R. D., Cuevas, E., García, O. E., Cachorro, V. E., Pallé, P., Bustos, J. J., Romero-Campos, P. M., and de Frutos, A. M.: Reconstruction of global solar radiation time series from 1933 to 2013 at the Izaña Atmospheric Observatory, Atmos. Meas. Tech., 7, 3139–3150, https://doi.org/10.5194/amt-7-3139-2014, 2014.

García, R. D., Cuevas, E., Ramos, R., Cachorro, V. E., Redondas, A., and Moreno-Ruiz, J. A.: Description of the Baseline Surface Radiation Network (BSRN) station at the Izaña Observatory (2009–2017): measurements and quality control/assurance procedures, Geosci. Instrum. Method. Data Syst., 8, 77–96, https://doi.org/10.5194/gi-8-77-2019, 2019.

Giles, D. M., Sinyuk, A., Sorokin, M. G., Schafer, J. S., Smirnov, A., Slutsker, I., Eck, T. F., Holben, B. N., Lewis, J. R., Campbell, J. R., Welton, E. J., Korkin, S. V., and Lyapustin, A. I.: Advancements in the Aerosol Robotic Network (AERONET) Version 3 database – automated near-real-time quality control algorithm with improved cloud screening for Sun photometer aerosol optical depth (AOD) measurements, Atmos. Meas. Tech., 12, 169–209, https://doi.org/10.5194/amt-12-169-2019, 2019.

Goloub, P., Li, Z., Dubovik, O., Blarel, L., Podvin, T., Jankowiak, I., Lecoq, R., Deroo, C., Chatenet, B., Morel, J., Cuevas, E., and Ramos, R.: PHOTONS/AERONET sunphotometer network overview: description, activities, results, in: Fourteenth International Symposium on Atmospheric and Ocean Optics/Atmospheric Physics, vol. 6936, p. 69360V, International Society for Optics and Photonics, 2007.

Grassl, H.: Calculated circumsolar radiation as a function of aerosol type, field of view, wavelength, and optical depth, Appl. Opt., 10, 2542–2543, https://doi.org/10.1364/AO.10.002542, 1971.

Gueymard, C.: SMARTS2: a simple model of the atmospheric radiative transfer of sunshine: algorithms and performance assessment, Florida Solar Energy Center Cocoa, FL, 1995.

Guirado, C., Cuevas, E., Cachorro, V. E., Toledano, C., Alonso-Pérez, S., Bustos, J. J., Basart, S., Romero, P. M., Camino, C., Mimouni, M., Zeudmi, L., Goloub, P., Baldasano, J. M., and de Frutos, A. M.: Aerosol characterization at the Saharan AERONET site Tamanrasset, Atmos. Chem. Phys., 14, 11753–11773, https://doi.org/10.5194/acp-14-11753-2014, 2014.

Holben, B., Eck, T., Slutsker, I., Tanré, D., Buis, J., Setzer, A., Vermote, E., Reagan, J., and Kaufman, Y.: Multi-band automatic sun and sky scanning radiometer system for measurement of aerosols, CNES, Proceedings of 6th International Symposium on Physical Measurements and Signatures in Remote Sensing, 75–83, 1994.

Holben, B., Eck, T., Slutsker, I., Tanré, D., Buis, J., Setzer, A., Vermote, E., Reagan, J., Kaufman, Y., Nakajima, T., Lavenu, F., Jankowiak, I., and Smirnov, A.: AERONET – A Federated Instrument Network and Data Archive for Aerosol Characterization, Remote Sens. Environ., 66, 1–16, https://doi.org/10.1016/S0034-4257(98)00031-5, 1998.

Holben, B. N., Tanré, D., Smirnov, A., Eck, T. F., Slutsker, I., Abuhassan, N., Newcomb, W. W., Schafer, J. S., Chatenet, B., Lavenu, F., Kaufman, Y. J., Vande Castle, J., Setzer, A.,Markham, B., Clark, D., Frouin, R., Halthore, R., Karneli, A., O'neill, N. T., Pietras, C., Pinker, C., Voss, K., and Zibordi, G.: An emerging ground-based aerosol climatology: Aerosol optical depth from AERONET, J. Geophys. Res.-Atmos., 106, 12067–12097, https://doi.org/10.1029/2001JD900014, 2001.

Huijnen, V. and Eskes, H.: Skill scores and evaluation methodology for the MACC II project, MACC-II Deliverable D_85, 2, availabel at: http://www.gmes-atmosphere.eu/documents/maccii/deliverables/val/MACCII_VAL_DEL_D_85.2_ScoringReport01_20120222.pdf (last access: 5 September 2018), 2012.

Huneeus, N., Basart, S., Fiedler, S., Morcrette, J.-J., Benedetti, A., Mulcahy, J., Terradellas, E., Pérez García-Pando, C., Pejanovic, G., Nickovic, S., Arsenovic, P., Schulz, M., Cuevas, E., Baldasano, J. M., Pey, J., Remy, S., and Cvetkovic, B.: Forecasting the northern African dust outbreak towards Europe in April 2011: a model intercomparison, Atmos. Chem. Phys., 16, 4967–4986, https://doi.org/10.5194/acp-16-4967-2016, 2016.

IPCC: The Physical Science Basis. Intergovernmental Panel on Climate Change, https://doi.org/10.1017/CBO9781107415324, 2013.

Jarosławski, J., Krzyścin, J. W., Puchalski, S., and Sobolewski, P.: On the optical thickness in the UV range: Analysis of the ground-based data taken at Belsk, Poland, J. Geophys. Res.-Atmos., 108, 4722, https://doi.org/10.1029/2003JD003571, 2003.

Kahn, R. A. and Gaitley, B. J.: An analysis of global aerosol type as retrieved by MISR, J. Geophys. Res.-Atmos., 120, 4248–4281, https://doi.org/10.1002/2015JD023322, 2015.

Kalnay, E., Kanamitsu, M., Kistler, R., Collins, W., Deaven, D., Gandin, L., Iredell, M., Saha, S., White, G., Woollen, J., Zhu, Y., Chelliah, M., Ebisuzaki, W., Higgins, W., Janowiak, J., Mo, K. C., Ropelewski, C., Wang, J., Leetmaa, A., Reynolds, R., Jenne, R., and Joseph, D.: The NCEP/NCAR 40-year reanalysis project, B. Am. Meteorol. Soc., 77, 437–472, 1996.

Kasten, F.: A new table and approximation formula for the relative optical air mass, Arch. Meteor. Geophy. B, 14, 206–223, https://doi.org/10.1007/BF02248840, 1966.

Kasten, F. and Young, A. T.: Revised optical air mass tables and approximation formula, Appl. Opt., 28, 4735–4738, https://doi.org/10.1364/AO.28.004735, 1989.

Kazadzis, S., Veselovskii, I., Amiridis, V., Gröbner, J., Suvorina, A., Nyeki, S., Gerasopoulos, E., Kouremeti, N., Taylor, M., Tsek-

eri, A., and Wehrli, C.: Aerosol microphysical retrievals from precision filter radiometer direct solar radiation measurements and comparison with AERONET, Atmos. Meas. Tech., 7, 2013–2025, https://doi.org/10.5194/amt-7-2013-2014, 2014.

Kazadzis, S., Kouremeti, N., Diémoz, H., Gröbner, J., Forgan, B. W., Campanelli, M., Estellés, V., Lantz, K., Michalsky, J., Carlund, T., Cuevas, E., Toledano, C., Becker, R., Nyeki, S., Kosmopoulos, P. G., Tatsiankou, V., Vuilleumier, L., Denn, F. M., Ohkawara, N., Ijima, O., Goloub, P., Raptis, P. I., Milner, M., Behrens, K., Barreto, A., Martucci, G., Hall, E., Wendell, J., Fabbri, B. E., and Wehrli, C.: Results from the Fourth WMO Filter Radiometer Comparison for aerosol optical depth measurements, Atmos. Chem. Phys., 18, 3185–3201, https://doi.org/10.5194/acp-18-3185-2018, 2018a.

Kazadzis, S., Kouremeti, N., Nyeki, S., Gröbner, J., and Wehrli, C.: The World Optical Depth Research and Calibration Center (WORCC) quality assurance and quality control of GAW-PFR AOD measurements, Geosci. Instrum. Method. Data Syst., 7, 39–53, https://doi.org/10.5194/gi-7-39-2018, 2018b.

Kentarchos, A., Roelofs, G., Lelieveld, J., and Cuevas, E.: On the origin of elevated surface ozone concentrations at Izana Observatory, Tenerife during late March 1996, Geophys. Res. Lett., 27, 3699–3702, https://doi.org/10.1029/2000GL011518, 2000.

Kim, S.-W., Jefferson, A., Soon-Chang, Y., Dutton, E., Ogren, J., Valero, F., Kim, J., and Holben, B.: Comparisons of aerosol optical depth and surface shortwave irradiance and their effect on the aerosol surface radiative forcing estimation, J. Geophys. Res.-Atmos., 110, D07204, https://doi.org/10.1029/2004JD004989, 2005.

Kim, S.-W., Yoon, S.-C., Kim, J., and Kim, S.-Y.: Seasonal and monthly variations of columnar aerosol optical properties over east Asia determined from multi-year MODIS, LIDAR, and AERONET Sun/sky radiometer measurements, Atmos. Environ., 41, 1634–1651, https://doi.org/10.1016/j.atmosenv.2006.10.044, 2007.

Kim, S.-W., Yoon, S.-C., Dutton, E., Kim, J., and Wehrli, C.and Holben, B.: Global surface-based sun photometer network for long-term observations of column aerosol optical properties: intercomparison of aerosol optical depth, Aerosol Sci. Tech., 42, 1–9, https://doi.org/10.1080/02786820701699743, 2008.

Klingmüller, K., Pozzer, A., Metzger, S., Stenchikov, G. L., and Lelieveld, J.: Aerosol optical depth trend over the Middle East, Atmos. Chem. Phys., 16, 5063–5073, https://doi.org/10.5194/acp-16-5063-2016, 2016.

Komhyr, W.: Dobson spectrophotometer systematic total ozone measurement error, Geophys. Res. Lett., 7, 161–163, 1980.

Komhyr, W. D., Grass, R. D., and Leonard, R. K.: Dobson spectrophotometer 83: A standard for total ozone measurements, 1962–1987, J. Geophys. Res.-Atmos., 94, 9847–9861, https://doi.org/10.1029/JD094iD07p09847, 1989.

Mahowald, N., Albani, S., Kok, J. F., Engelstaeder, S., Scanza, R., Ward, D. S., and Flanner, M. G.: The size distribution of desert dust aerosols and its impact on the Earth system, Aeolian Res., 15, 53–71, https://doi.org/10.1016/j.aeolia.2013.09.002, 2014.

McArthur, L. J. B., Halliwell, D. H., Niebergall, O. J., O'Neill, N. T., Slusser, J. R., and Wehrli, C.: Field comparison of network Sun photometers, J. Geophys. Res.-Atmos., 108, 4596, https://doi.org/10.1029/2002JD002964, 2003.

McPeters, R. D., Frith, S., and Labow, G. J.: OMI total column ozone: extending the long-term data record, Atmos. Meas. Tech., 8, 4845–4850, https://doi.org/10.5194/amt-8-4845-2015, 2015.

Mitchell, R. and Forgan, B.: Aerosol measurement in the Australian outback: Intercomparison of sun photometers, J. Atmos. Ocean. Tech., 20, 54–66, https://doi.org/10.1175/1520-0426(2003)020<0054:AMITAO>2.0.CO;2, 2003.

Mitchell, R. M., Forgan, B. W., and Campbell, S. K.: The Climatology of Australian Aerosol, Atmos. Chem. Phys., 17, 5131–5154, https://doi.org/10.5194/acp-17-5131-2017, 2017.

Nakajima, T., Yoon, S.-C., Ramanathan, V., Shi, G.-Y., Takemura, T., Higurashi, A., Takamura, T., Aoki, K., Sohn, B.-J., Kim, S.-W., Tsuruta, H., Sugimoto, N., Shimizu, A., Tanimoto, H., Sawa, Y., Lin, N.-H., Lee, C.-T., Goto, D., and Schutgens, N.: Overview of the Atmospheric Brown Cloud East Asian Regional Experiment 2005 and a study of the aerosol direct radiative forcing in east Asia, J. Geophys. Res.-Atmos., 112, D24S91, https://doi.org/10.1029/2007JD009009, 2007.

Nyeki, S., Halios, C., Baum, W., Eleftheriadis, K., Flentje, H., Gröbner, J., Vuilleumier, L., and Wehrli, C.: Ground-based aerosol optical depth trends at three high-altitude sites in Switzerland and southern Germany from 1995 to 2010, J. Geophys. Res.-Atmos., 117, D18202, https://doi.org/10.1029/2012JD017493, 2012.

Nyeki, S., Gröbner, J., and Wehrli, C.: Ground-based aerosol optical depth inter-comparison campaigns at European EU-SAAR super-sites, in Radiation Processes in the Atmosphere and Ocean (IRS2012), AIP Conf. Proc., 1531, 584–587, https://doi.org/10.1063/1.4804837, 2013.

Nyeki, S., Wehrli, C., Gröbner, J., Kouremeti, N., Wacker, S., Labuschagne, C., Mbatha, N., and Brunke, E.-G.: The GAW-PFR aerosol optical depth network: The 2008–2013 time series at Cape Point Station, South Africa, J. Geophys. Res.-Atmos., 120, 5070–5084, 2015.

Räisänen, P. and Lindfors, A. V.: On the computation of apparent direct solar radiation, J. Atmos. Sci., https://doi.org/10.1175/JAS-D-19-0030.1, 2019.

Räisänen, P., Isaac, G. A., Barker, H. W., and Gultepe, I.: Solar radiative transfer for stratiform clouds with horizontal variations in liquid-water path and droplet effective radius, Q. J. Roy. Meteor. Soc., 129, 2135–2149, https://doi.org/10.1256/qj.02.149, 2003.

Rodríguez, S., González, Y., Cuevas, E., Ramos, R., Romero, P. M., Abreu-Afonso, J., and Redondas, A.: Atmospheric nanoparticle observations in the low free troposphere during upward orographic flows at Izaña Mountain Observatory, Atmos. Chem. Phys., 9, 6319–6335, https://doi.org/10.5194/acp-9-6319-2009, 2009.

Rodríguez, S., Alastuey, A., Alonso-Pérez, S., Querol, X., Cuevas, E., Abreu-Afonso, J., Viana, M., Pérez, N., Pandolfi, M., and de la Rosa, J.: Transport of desert dust mixed with North African industrial pollutants in the subtropical Saharan Air Layer, Atmos. Chem. Phys., 11, 6663–6685, https://doi.org/10.5194/acp-11-6663-2011, 2011.

Rodríguez, S., Cuevas, E., Prospero, J. M., Alastuey, A., Querol, X., López-Solano, J., García, M. I., and Alonso-Pérez, S.: Modulation of Saharan dust export by the North African dipole, Atmos. Chem. Phys., 15, 7471–7486, https://doi.org/10.5194/acp-15-7471-2015, 2015.

Rodriguez-Franco, J. J. and Cuevas, E.: Characteristics of the sub-tropical tropopause region based on long-term highly resolved sonde records over Tenerife, J. Geophys. Res.-Atmos., 118, 10–754, https://doi.org/10.1002/jgrd.50839, 2013.

Romero, P. M. and Cuevas, E.: Variación diurna del espesor óptico de aerosoles: ¿ficción o realidad?, 3 Asamblea Hispano Portuguesa de Geofísica y Geodesia, Valencia, 2002.

Romero-Campos, P., Cuevas, A., Kazadzis, S., Kouremeti, N., García, R., and Guirado-Fuentes, C.: Análisis de la trazabilidad en los valores del AOD obtenidos a partir de las medidas de las redes AERONET-CIMEL y GAW-PFR durante el período 2005–2015 en el Observatorio Atmosférico de Izaña, 2017.

Russell, P., Livingston, J., Dubovik, O., Ramirez, S., Wang, J., Redemann, J., Schmid, B., Box, M., and Holben, B.: Sunlight transmission through desert dust and marine aerosols: Diffuse light corrections to Sun photometry and pyrheliometry, J. Geophys. Res.-Atmos., 109, D08207, https://doi.org/10.1029/2003JD004292, 2004.

Sakerin, S. M., Kabanov, D., Panchenk, M., Pol'kin, V., Holben, B., Smirnov, A., Beresnev, S., Gorda, S., Kornienko, G., Nikolashkin, S., Poddubnyi, V., and Tashchilin, M.: Monitoring of atmospheric aerosol in the Asian part of Russia in 2004 within the framework of AEROSIBNET program, Atmos. Ocean. Opt., 18, 871–878, 2005.

Sayer, A. M., Hsu, N. C., Bettenhausen, C., Jeong, M.-J., Holben, B. N., and Zhang, J.: Global and regional evaluation of over-land spectral aerosol optical depth retrievals from SeaWiFS, Atmos. Meas. Tech., 5, 1761–1778, https://doi.org/10.5194/amt-5-1761-2012, 2012.

Sayer, A. M., Hsu, N. C., Bettenhausen, C., and Jeong, M.: Validation and uncertainty estimates for MODIS Collection 6 "Deep Blue" aerosol data, J. Geophys. Res.-Atmos., 118, 7864–7872, https://doi.org/10.1002/jgrd.50600, 2013.

Schmid, B. and Wehrli, C.: Comparison of Sun photometer calibration by use of the Langley technique and the standard lamp, Appl. Opt., 34, 4500–4512, https://doi.org/10.1364/AO.34.004500, 1995.

Schmid, B., Michalsky, J., Halthore, R., Beauharnois, M., Harrison, L., Livingston, J., Russell, P., Holben, B., Eck, T., and Smirnov, A.: Comparison of aerosol optical depth from four solar radiometers during the fall 1997 ARM intensive observation period, Geophys. Res. Lett., 26, 2725–2728, https://doi.org/10.1029/1999GL900513, 1999.

Sinyuk, A., Holben, B. N., Smirnov, A., Eck, T. F., Slutsker, I., Schafer, J. S., Giles, D. M., and Sorokin, M.: Assessment of error in aerosol optical depth measured by AERONET due to aerosol forward scattering, Geophys. Res. Lett., 39, L25806, https://doi.org/10.1029/2012GL053894, 2012.

Smirnov, A., Holben, B., Eck, T., Dubovik, O., and Slutsker, I.: Cloud-screening and quality control algorithms for the AERONET database, Remote Sens. Environ., 73, 337–349, https://doi.org/10.1016/S0034-4257(00)00109-7, 2000.

Takamura, T. and Nakajima, T.: Overview of SKYNET and its activities, Opt. Pura Apl., 37, 3303–3308, 2004.

Thomason, L., Herman, B. M., Schotland, R. M., and Reagan, J. A.: Extraterrestrial solar flux measurement limitations due to a Beer's law assumption and uncertainty in local time, Appl. Opt., 21, 1191–1195, https://doi.org/10.1364/AO.21.001191, 1982.

Todd, M. C., Washington, R., Martins, J. V., Dubovik, O., Lizcano, G., M'bainayel, S., and Engelstaedter, S.: Mineral dust emission from the Bodélé Depression, northern Chad, during BoDEx 2005, J. Geophys. Res.-Atmos., 112, D06207, https://doi.org/10.1029/2006JD007170, 2007.

Toledano, C., Cachorro, V. E., Berjón, A., de Frutos, A. M., Sorribas, M., de la Morena, B. A., and Goloub, P.: Aerosol optical depth and Ångström exponent climatology at El Arenosillo AERONET site (Huelva, Spain), Q. J. Roy. Meteor. Soc., 133, 795–807, https://doi.org/10.1002/qj.54, 2007.

Toledano, C., Cachorro, V. E., Berjón, A., de Frutos, A. M., Fuertes, D., González, R., Torres, B., Rodrigo, R., Bennouna, Y., Martin, L., and Guirado, C.: RIMA-AERONET network: long term monitoring of aerosol properties, Opt. Pura Apl., 44, 629–633, 2011.

Toledano, C., Cachorro, V., Gausa, M., Stebel, K., Aaltonen, V., Berjón, A., de Galisteo, J. P. O., de Frutos, A. M., Bennouna, . Y., Blindheim, S., Myhre, C. L., Zibordi, G., Wehrli, C., Kratzer, S., Hakansson, B., Carlund, T., de Leeuw, G., Herber, A., and Torres, B.: Overview of Sun Photometer Measurements of Aerosol Properties in Scandinavia and Svalbard, Atmos. Environ., 52, 18–28, https://doi.org/10.1016/j.atmosenv.2011.10.022, 2012.

Toledano, C., González, R., Fuertes, D., Cuevas, E., Eck, T. F., Kazadzis, S., Kouremeti, N., Gröbner, J., Goloub, P., Blarel, L., Román, R., Barreto, Á., Berjón, A., Holben, B. N., and Cachorro, V. E.: Assessment of Sun photometer Langley calibration at the high-elevation sites Mauna Loa and Izaña, Atmos. Chem. Phys., 18, 14555–14567, https://doi.org/10.5194/acp-18-14555-2018, 2018.

Torres, B., Toledano, C., Berjón, A., Fuertes, D., Molina, V., Gonzalez, R., Canini, M., Cachorro, V. E., Goloub, P., Podvin, T., Blarel, L., Dubovik, O., Bennouna, Y., and de Frutos, A. M.: Measurements on pointing error and field of view of Cimel-318 Sun photometers in the scope of AERONET, Atmos. Meas. Tech., 6, 2207–2220, https://doi.org/10.5194/amt-6-2207-2013, 2013.

Wagner, F. and Silva, A. M.: Some considerations about Ångström exponent distributions, Atmos. Chem. Phys., 8, 481–489, https://doi.org/10.5194/acp-8-481-2008, 2008.

Wang, J., Xia, X., Wang, P., and Christopher, S.: Diurnal variability of dust aerosol optical thickness and Ångström exponent over dust source regions in China, Geophys. Res. Lett., 31, L08107, https://doi.org/10.1029/2004GL019580, 2004.

Wehrli, C.: Calibrations of filter radiometers for determination of atmospheric optical depth, Metrologia, 37, 419, https://doi.org/10.1088/0026-1394/37/5/16, 2000.

Wehrli, C.: GAWPFR: A network of aerosol optical depth observations with precision filter radiometers, GLOBAL ATMOSPHERE WATCH, p. 36, 2005.

Wehrli, C.: Precision Filter Radiometer Documentation, Version 4.0, 38 pp., Davos Dorf, 2008a.

Wehrli, C.: Remote sensing of aerosol optical depth in a global surface network, PhD thesis, ETH Zurich, available at: https://www.research-collection.ethz.ch/bitstream/handle/20.500.11850/150574/eth-30693-02.pdf (last access: 1 September 2018), 2008b.

Weinzierl, B., Sauer, D., Esselborn, M., Petzold, A., Veira, A., Rose, M., Mund, S., Wirth, M., Ansmann, A., Tesche, M., Gross, S., and Freudenthaler, V.: Microphysical and optical properties of dust and tropical biomass burning aerosol layers in the

Cape Verde region – an overview of the airborne in situ and lidar measurements during SAMUM-2, Tellus B, 63, 589–618, https://doi.org/10.1111/j.1600-0889.2011.00566.x, 2011.

WMO: Recent Progress in Sunphotometry, Determination of the aerosol optical depth, Environmental Pollution Monitoring and Research Programme, No. 43, 21 pp., November, 1986.

WMO: Aerosol measurement procedures, guidelines and recommendations, GAW Report No. 153, WMO TD No. 1178, avaible at: https://library.wmo.int/pmb_ged/wmo-td_1178.pdf (last access: 1 September 2018), 2003.

WMO: WMO/GAW Experts Workshop on a Global Surface-Based Network for Long Term Observations of Column Aerosol Optical Properties, GAW Report No. 162, WMO TD No. 1287, available at: https://library.wmo.int/pmb_ged/wmo-td_1287.pdf (last access: 1 September 2018), 2005.

WMO: Abridged final report with resolutions and recommendations, GAW Report WMO TD No. 1019, WMO-CIMO Fourteenth session Geneva 7–14 December 2006, 2007.

WMO: Commission for Instruments and Methods of Observation, Sixteenth session WMO no.1138, Saint Petersburg, Secretariat of the World Meteorological Organization, 2014.

WMO: Aerosol Measurement Procedures, Guidelines and Recommendations, 2nd Edition, WMO No 1177, 2016.

Young, A. T.: Revised depolarization corrections for atmospheric extinction, Appl. Opt., 19, 3427–3428, https://doi.org/10.1364/AO.19.003427, 1980.